AD-A105 635 FOREIGN TECHNOLOGY DIV WRIGHT-PATTERSON AFB OH F/G 20/4
ACTA MECHANICA SINICA (SELECTED ARTICLES).(U)
SEP 81
UNCLASSIFIED FTD-ID(RS)T-0705-81 NL

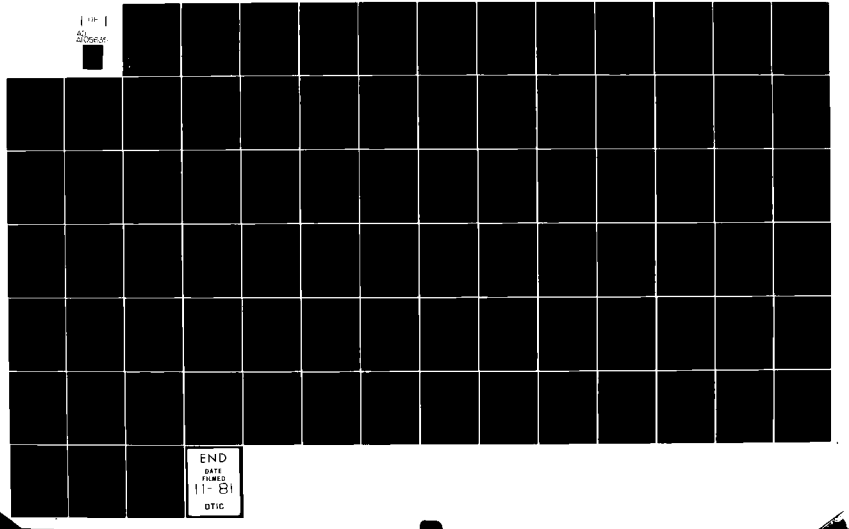

END
DATE FILMED
11-81
DTIC

FTD-ID(RS)T-0795-81

AD A105635

FOREIGN TECHNOLOGY DIVISION

ACTA MECHANICA SINICA
(Selected Articles)

Approved for public release;
distribution unlimited.

81 10 7 170

EDITED TRANSLATION

(14) FTD-ID(RS)T-0705-81 (11) 15 September 1981

MICROFICHE NR: FTD-81-C-000842

(6) ACTA MECHANICA SINICA (Selected Articles). (12) 85

English pages: 83

Source: Acta Mechanica Sinica, Nr. 2, 1979, pp. 129-157, 171-177, 182-185, 193-198

Country of origin: China
Translated by: SCITRAN
F33657-78-D-0619
Requester: FTD/TQTA

PREPARED BY:

TRANSLATION DIVISION
FOREIGN TECHNOLOGY DIVISION
WP-AFB, OHIO.

744600 slh

TABLE OF CONTENTS

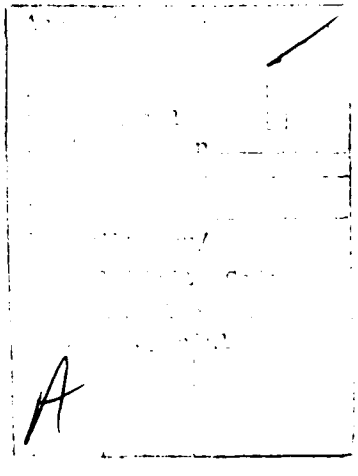

DIFFERENCE METHOD IN FLUID DYNAMICS

I. NUMERICAL SOLUTION OF TWO-DIMENSIONAL VORTICITY EQUATION

Guo Benyu

Shanghai University of Science and Technology

ABSTRACT

With the two-dimensional vorticity equation as an example, this paper systematically discussed the theoretical problem of difference equations in fluid dynamics. Many schemes are constructed in this paper based on the conservation laws and transport properties. Generalized stability is introduced. The error of periodic solutions is rigorously estimated. The effect of error in boundary values on the stability of computation and the boundary shape, boundary conditions and its treatment in the initial/boundary problems are analyzed. The computational problem of non-viscous flow and large gradient solution is treated according to the conservation laws. Lastly, the convergence of dynamic relaxation and the existence of solutions of steady flow computational schemes are studied. All the results in this paper are proved rigorously, and the method used is also applicable to the general fluid dynamic problems. Examples are used to illustrate the applications of these results in fluid dynamic computations and numerical weather forecast.

The theoretical study of difference method basically consists of five aspects: (1) the principles of scheme; (2) stability of solution against perturbation on the RHS and the initial values; (3) non-viscous flow calculation; (4) effect of boundary shape, type of boundary condition, and error in boundary value on the solution of initial/boundary value problems; (5) steady flow calculation [1-5]. A large amount of work has been done in foreign countries but there are only a few very special theoretical results. Based on the work of Ref. [6-8], we discuss in this paper all aspects of the five problems quoted above with the two-dimensional vorticity equation as an example, and obtain a more systematic result. The method is applicable to the general fluid dynamical problems.

I. Symbols and Lemmas

R represents an open region in (x_1, x_2) plane with boundary Γ. The grid step length along x_j direction is h. The coordinates of the grid point Q are $x_j(Q) = k_j(Q)h$, where $k_j(Q)$ is an integer. The coordinate of $k_j(Q)$ is $k_j(Q^{\pm e_j}) = k_j(Q) \pm \delta_{j,\cdots}$ R_h represents the set of internal grid points with boundary Γ_h. Γ_{jM} (or Γ_{jm}) is the set of boundary points that makes Q^{-e_j} (or Q^{+e_j}) belong to R_h. R_{jM} (or R_{jm}) represents the set of all internal points at distance h from Γ_{jM} (or Γ_{jm}). $\Gamma_j = \Gamma_{jM} + \Gamma_{jm}$, $R_j = R_{jM} + R_{jm}$, $R_h^* = R_h + R_h$. τ is the step length along τ, $\lambda = \tau h^{-1}$, $w(Q, k)$ represents the value of the net function w at time $k\tau$ and position Q. Sometimes it is simply denoted by $w(Q)$, $w(k)$ or w, $\bar{w} = \bar{w}(k) = w(k+1)$. w_{x_j}, $w_{\bar{x}_j}$, represents the forward, backward and central difference coefficients along x_j. $w_n(Q)$ is the outer normal difference coefficient on R_h^*. When $Q \in R_{jM}$, $w_n(Q) = w_{x_j}(Q)$. When $Q \in R_{jm}$, $w_n(Q) = -w_{\bar{x}_j}(Q)$. represents the tangential difference coefficient on $R_h^* + \Gamma_h$. When $Q \in R_{jM} + \Gamma_{jM}$, $w_\tau(Q) = w_{\bar{x}_j}(Q)$, . When $Q \in R_{jm} + \Gamma_{jm}$,

$w_1(Q) = -w_{2_1}(Q)$. When $Q \in R_{2M} + \Gamma_{1M}$, $w_1(Q) = -w_{2_1}(Q)$. When $Q \in R_{2m} + \Gamma_{1m}$, $w_1(Q) = w_{2_1}(Q)$.

If $Q \in R_h^*$, we shall denote by Q^1 the point on Γ_h at distance h from Q, and also denote $\sum_{Q \in R_h^*} [w(Q')v(Q) + w(Q)v(Q')]$ simply as $\sum_{R_h^*}' (w'v + wv')$, etc.

We further define /130

$$\Delta_i^* w = \frac{1}{2}(\nu w_{x_i})_{\bar{x}_i} + \frac{1}{2}(\nu w_{\bar{x}_i})_{x_i}, \quad \Delta^* w = \sum_{i=1}^{s} \Delta_i^* w$$

Denote $\nu^{\pm s_i} = \nu(Q^{\pm s_i})$, $H^*(w) = H_i^*(w)$ is an ADE type operator, i.e. is taken according to a certain order, where

$$H_1^*(w) = -\frac{1}{2}(\nu + \nu^{-s_1})w_{1s_1} - \frac{1}{2}(\nu + \nu^{-s_2})w_{1s_2}$$

$$H_2^*(w) = \frac{1}{2}(\nu + \nu^{+s_1})w_{1s_1} - \frac{1}{2}(\nu + \nu^{-s_2})w_{1s_2}$$

$$H_3^*(w) = -\frac{1}{2}(\nu + \nu^{-s_1})w_{1s_1} + \frac{1}{2}(\nu + \nu^{+s_2})w_{1s_2}$$

$$H_4^*(w) = \frac{1}{2}(\nu + \nu^{+s_1})w_{1s_1} + \frac{1}{2}(\nu + \nu^{+s_2})w_{1s_2}$$

We define the following internal products and norms:

$$(w, v) = \sum_{Q \in R_h} h^2 w(Q)v(Q), \quad \|w\|^2 = (w, w)$$

$\|w\|_{\nu}^2 = \frac{1}{2}\sum_{i=1}^{s}(\|\sqrt{\nu}\, w_{x_i}\|^2 + \|\sqrt{\nu}\, w_{\bar{x}_i}\|^2)$, if $\nu \equiv 1$, then simply denote by $\|w\|_1^2$.

$$\|w\|_1^2 = \frac{1}{2}\sum_{i=1}^{s}(\|w_{x_i}\|_1^2 + \|w_{\bar{x}_i}\|_1^2), \quad \|w\|_{\Gamma_h}^2 = \sum_{Q \in \Gamma_h} h w^2(Q)$$

Denote also

$$B_{kj}(u, v, w) = \frac{h}{2}\sum_{R_j}(u'v + uv')w, \quad B_{R_h^*}(u, v, w) = \sum_{j=1}^{3} B_{R_j}(u, v, w)$$

$$D_*(w) = \sum_{R_{1M}+R_{2M}}\left(\frac{\nu}{2}w'^2 - \nu w w' - \frac{\nu'}{2}w^2\right)$$

$$- \sum_{R_{1m}+R_{2m}}\left(\frac{\nu'}{2}w^2 - \nu' w w' - \frac{\nu}{2}w'^2\right)$$

$$B_{\sigma m\theta}(w) = \|w\|_1^2 + \tau\left(\sigma + \frac{m}{2}\right)(\|w\|_{1\nu}^2)_t - \theta\tau\|w_t\|^2 + \theta\tau\|w\|_{21}^2$$

$$+ \frac{m\theta\tau^2}{2}\|w_t\|_1^2 + p_1\tau^2\|w_t\|_{1\nu}^2 + p_2\tau\|w_t\|^2$$

where

$$p_1 = \sigma m - \frac{m}{2} - \sigma + \frac{\chi m}{2}, \quad p_2 = m - 1 - \theta$$

$$\|w(k)\|_{\hat{w}\nu}^2 = \|w(k)\|^2 + \tau\sum_{j=0}^{k-1}\|w(j)\|_{1\nu}^2$$

$$\rho(w, f_1, f_2, g, k) = \|w(0)\|^2 + \tau\sum_{j=0}^{k}(\|f_1(j)\|^2 + \|f_2(j)\|^2 + \|g(j)\|_{1h}^2)$$

It can be proved that

$$2(w, w_t) = (\|w\|^2)_t - \tau\|w_t\|^2 \tag{1.1}$$

$$2(w, w_t) = (\|w\|^2)_t + \tau\|w_t\|^2 \tag{1.2}$$

/131

$$2(w, w_{tt}) = \|w\|_{21}^2 - \|w_t\|^2 - \|w_t\|^2 \tag{1.3}$$

(1.4)

$$2(u\ \Delta^*_{\cdot,\cdot}) + (\nu w_{x_1}, v_{x_1}) + (\nu w_{x_2}, v_{x_2}) - 2B_{R_j}(v, w, v_x) = 0$$

$$(w, \Delta^* w) + \|w\|_{1\nu}^2 - B_{R_h^*}(v, w, w_x) = 0 \tag{1.5}$$

$$2(w_t, \Delta^* w) + (\|w\|_{1\nu}^2)_t - \tau\|w_t\|_{1\nu}^2 - \frac{1}{2}\sum_{j=1}^{2}(\nu_{x_j}, \bar{w}_{x_j}^2 + \bar{w}_{x_j}^2)$$

$$- 2B_{R_h^*}(v, w_t, w_x) = 0 \tag{1.6}$$

$$2(w, \Delta^* w_t) + (\|w\|_{1\nu}^2)_t - \tau\|w_t\|_{1\nu}^2 - \frac{1}{2}\sum_{j=1}^{2}(\nu_{x_j}, \bar{w}_{x_j}^2 + \bar{w}_{x_j}^2) \tag{1.7}$$

$$- 2B_{R_h^*}(v, w, w_{tx}) = 0$$

$$2(w_t, H^h(w)) + h\|w_t\|_v^2 - \sum_{i=1}^{2}(\nu_{x_i}, w_i^2) - hD_v(w_t) = 0 \tag{1.8}$$

Lemma 1. If $q > r > 0$, , then $\|w^q\|^2 \leqslant \|w^r\|^{\frac{2q}{r}} h^{2(1-\frac{q}{r})}$.

Lemma 2. If $w|_{\Gamma_1} = v|_{\Gamma_1} = 0$, then $\|wv\|^2 \leqslant 4\|w\|\|v\|\|w\|_1\|v\|_1$.

Lemma 3. If $w|_{\Gamma_h} = 0$, then $\|w\|_1^2 \leqslant \|\Delta w\|^2$.

Lemma 4. Assume: (1) $w(k)$, $v(k)$ is a non-negative net function. $\rho(T)$ is non-negative, τ is suitable small, M_0, $\ldots p \geqslant 0$; (2) $H_w(k) = c_0 w(k)|p + w(k)h^{-\alpha_1}| + f^*[w(k)]v(k)$, $s \leqslant M_0 h^{-\alpha_1}$, $f^*(s) \leqslant 0$; (3) $w(0) \leqslant \frac{1}{2}\rho(T)$, when $1 \leqslant k \leqslant \left[\frac{T}{\tau}\right]$; $w(k) \leqslant \rho(T) + \tau\sum_{i=0}^{k-1} H_w(i)$; (4)

$\rho e^{\lambda_0 \rho' t_0} \leqslant \ldots p h^{-\ldots} M_0 h^{-\alpha_1})$, then when $k\tau \leqslant T \leqslant T_0$, $w(k) \leqslant \rho e^{\lambda_0 \rho T}$.

II. Basic Principles of Scheme Construction

Let $\xi(x_1, x_2, t)$ and $\psi(x_1, x_2, t)$ represent vorticity and flow function. Then the 2 dimensional vorticity equation is

$$\left.\begin{aligned} &\frac{\partial \xi}{\partial t} - \frac{\partial \psi}{\partial x_2}\frac{\partial \xi}{\partial x_1} + \frac{\partial \psi}{\partial x_1}\frac{\partial \xi}{\partial x_2} - \sum_{i=1}^{2}\frac{\partial}{\partial x_i}\left(\nu\frac{\partial \xi}{\partial x_i}\right) = f_1, && R \times [0, T] \\ &\nabla^2\psi - \xi = f_2, && R \times [0, T] \end{aligned}\right\} \tag{2.1}$$

Where $f_1(x_1, x_2, t)$ is known, $\nu(x_1, x_2, t)$ is coefficient of viscosity, $0 < \nu_0 \leqslant \nu \leqslant \nu_1$. We also denote

$$\nu_0 = \inf_{Q \in R_h^0 + \Gamma_h} \nu(Q), \quad s^* = \sup_{Q, Q' \in R_h^0} \nu(Q)\nu^{-1}(Q')$$

and assume $\left|\frac{\partial \nu}{\partial x_i}\right|$ and $\left|\frac{\partial \nu}{\partial t}\right|$ are bounded.

The principle of scheme construction is to express physical laws with suitable separation form, for example, if $\nu \equiv f_1 = 0$, then we get from (2.1) the conservation laws for vorticity and its square:

$$F'(\xi, t) = \iint_R \xi'(x_1, x_2, t)dx_1dx_2 = \iint_R \xi'(x_1, x_2, 0)dx_1dx_2$$

$$+\int_{\tau_1}^{\tau_2}\int_{\Gamma_1}\xi^i\left(\frac{\partial\psi}{\partial x_1}dx_1+\frac{\partial\psi}{\partial x_2}dx_2\right)d\tau \qquad i=1,2$$

As for the difference scheme, since the step length is non-zero, we cannot simultaneously simulate both conservation laws. The E_1 conservation law is simulated by the Lax scheme. We[6-8] simulate the E_2 conservation property. Let us define

$$\begin{aligned}
&J^+_{x_1,1}(v,w)=v_{x_1}w_{x_1}, && J^-_{x_1,1}(v,w)=v_{x_1}w_{x_1},\\
&J^+_{x_1,2}(v,u)=(vw_{x_1})_{x_1}, && J^-_{x_1,2}(v,w)=(vw_{x_1})_{x_1},\\
&J^+_{x_1,3}(v,w)=-(v_{x_1}w)_{x_1}, && J^-_{x_1,3}(v,w)=-(v_{x_1}w)_{x_1},\\
&J^+_{x_2,1}(v,w)=-v_{x_2}w_{x_2}, && J^-_{x_2,1}(v,w)=-v_{x_2}w_{x_2},\\
&J^+_{x_2,2}(v,w)=-(vw_{x_2})_{x_2}, && J^-_{x_2,2}(v,w)=-(vw_{x_2})_{x_2},\\
&J^+_{x_2,3}(v,w)=(v_{x_2}w)_{x_2}, && J^-_{x_2,3}(v,w)=(v_{x_2}w)_{x_2}.
\end{aligned}$$

$$J_{x_j,i}(v,w)=\frac{1}{2}J^+_{x_j,i}(v,w)+\frac{1}{2}J^-_{x_j,i}(v,w)$$

$$J^+_i(v,w)=\sum_{j=1}^{3}J^+_{x_j,i}(v,w), \qquad J^-_i(v,w)=\sum_{j=1}^{3}J^-_{x_j,i}(v,w)$$

$$J_i(v,w)=\frac{1}{2}J^+_i(v,w)+\frac{1}{2}J^-_i(v,w)$$

$$J^+(v,w)=\sum_{i=1}^{3}\alpha_iJ^+_i(v,w), \qquad J^-(v,w)=\sum_{i=1}^{3}\alpha_iJ^-_i(v,w)$$

$$J_{x_j}(v,w)=\sum_{i=1}^{3}\alpha_iJ_{x_j,i}(v,w), \qquad J(v,w)=\sum_{i=1}^{2}J_{x_i}(v,w)$$

where $\alpha_i\geq 0,\ \sum_{i=1}^{3}\alpha_i=1$. It can be proved that

$$(u,J_{x_j,1}(v,u))+(v,J_{x_j,2}(u,w))=B_{R_j}(uw_{x_j},v,1) \tag{2.2}$$

$$(u,J_1(v,u))+(v,J_2(u,w))=-B_{R_0^*}(u,wv_{x_1},1)-B_{R_0^*}(v,wu_{x_1},1) \tag{2.3}$$

If $\alpha_1=\alpha_2$, then

$$\begin{aligned}(u,J(v,w))+(v,J(u,w))&=\alpha_1B_{R_0^*}(uw_{x_1},v,1)+\alpha_1B_{R_0^*}(vw_{x_1},u,1)\\&-\alpha_2B_{R_0^*}(u,wv_{x_1},1)-\alpha_3B_{R_0^*}(v,wu_{x_1},1)\end{aligned} \tag{2.4}$$

If one the the 2 following conditions are satisfied on the boundary Γ_h :

A. The various quantities are periodic with periodicity L_1, R_h along the direction x_i . R_h is the rectangle $[0, L_1 - h; 0, L_2 - h]$;

B. R_h is a limited region and the flow along Γ_h is zero. For example, $u = v = w = 0$, then the RHS of equation (2.4) is zero. If we now use η, φ and $J(\eta, \varphi)$ to approximate ξ, ψ and the Jacobi operator in equation (2.1), then when $\alpha_1 = \alpha_2$, the conservation law

$$(\eta, J(\eta, \varphi)) = \alpha_1 B_{k_h^*}(\eta\varphi_1, \eta, 1) - \alpha_2 B_{k_h^*}(\eta, \varphi\eta_1, 1) \tag{2.5}$$

is well described.

If condition A or B is satisfied on the boundary, and $\alpha_1 = \alpha_2 = \frac{1}{2}$, then

$$(\eta, J_{x_i}(\eta, \varphi)) = 0 \tag{2.6}$$

The weighted average conservative scheme for computing equation (2.1) is

$$\left.\begin{aligned} &L_1(\eta, \varphi) \equiv \eta + \theta\tau\eta_{\bar{t}} - J(\eta + \delta\tau\eta_{\bar{t}}, \varphi) - \Delta^*(\eta + \sigma\tau\eta_{\bar{t}}) - \chi\tau h^{-1}H^*(\eta) = f_1 \\ &L_2(\eta, \varphi) = \Delta\varphi - \eta = f_2 \end{aligned}\right\} \tag{2.7}$$

/133

where $0 \leqslant \sigma_0 \leqslant \sigma(k) \leqslant \sigma_1 \leqslant 1, 0 \leqslant \delta(k) \leqslant 1, 0 \leqslant \chi(k) \leqslant 1, -\frac{1}{2} < \theta(k) \leqslant 0$, but when $\eta^{(1)}$ is calculated, we always take $\theta(0) = 0$. In the explanation below, we might as well assume that condition A is satisfied.

1. The function of δ is to maintain the conservative property. If fact, if $\nu = f_1 = \theta = \chi = \delta = 0, \alpha_1 = \alpha_2$, we still have $\|\eta\|_1^2 = \tau\|\eta_{\bar{t}}\|^2$. Hence each step of the computation will

see a small increase of the virtual energy which will cause energy explosion and computational overflow when it exceeds some critical value through long term accumulation. But if $\theta = 1/2$, then $\|\eta\|_1^2 = 0$ and the conservation is strict.

2. The function of θ is to filter. It equivalently filters the η in η_1 to be $\eta^* = \eta - \tau^2\theta\eta_{xx}$. If the harmonic function of the computer error $\bar{\eta}(k) = Ae^{ikx}$, then

$$\bar{\eta}^*(k) = \left(1 + 4\theta\sin^2\frac{k\tau}{2}\right)\bar{\eta}(k)$$

Because $-\frac{1}{2} < \theta \leqslant 0$, hence $\|\bar{\eta}^*\| \leqslant \|\bar{\eta}\|$, so that its growth is suppressed. Robert has used explicit filtering and $\theta = -0.01$. See [14].

3. If $\chi \neq 0$, then equation (2.7) is the successive overrelaxation scheme which is used to improve computational stability. Usually the $H_i^n(\eta)$ are used in turn to obtain η_i, and then let

$$\eta = \frac{1}{4}\sum_{i=1}^{4}\eta_i$$

which is the Larkin method[1].

4. In (2.7) we can also use the linear combination of f_1 and f_1 to replace f_i . All the results in this paper will also hold.

The weighted average conservation method may be used in conjunction with the splitting method, namely with η* as the supplement value.

$$\left.\begin{aligned}\eta^* &= \eta + \frac{\tau}{2}J_{x_1}(\eta+\eta^*,\varphi) + \frac{\tau}{2}\Delta_{x_1}^2(\eta+\eta^*) + \frac{\tau}{2}f_i\\ \eta &= \eta^* + \frac{\tau}{2}J_{x_2}(\eta^*+\eta,\varphi) + \frac{\tau}{2}\Delta_{x_2}^2(\eta^*+\eta) + \frac{\tau}{2}f_i\end{aligned}\right\} \qquad (2.8)$$

If $f_1 = \nu = 0, \alpha_1 = \alpha_2 = \frac{1}{2}$, then from equation (2.6), $\|\eta\|^2 = \|\eta\|^2$. Since equation (2.8) not only strictly satisfies the conservation laws, but also may be computed explicitly, it is to be recommended.

Another principle for scheme construction is the transport property. Let Q be an internal net point. Form tne triangle D_1 with $Q, Q^{+\tau_1}, Q^{+\tau_2}$ as the vertices, D_2, with $Q, Q^{+\tau_1}, Q^{-\tau_2}$ as vertices, and similarly for D_3, D_4 . If $\varphi_{x_1} \leqslant 0$, $\varphi_{x_2} \leqslant 0$, then the wind blows toward Q in D_1 . Denote it by $\varepsilon(D_1, \varphi) = 1$ else $\varepsilon(D_1, \varphi) = 0$. Similarly the other $\varepsilon(D_i, \varphi)$ may be computed. We shall construct the difference operator $F(\eta, \varphi)$ for the following three cases:

1. $\varepsilon(D_i, \varphi) = \delta_{i0}$, indicating that the wind blows unidirectionally toward Q. For example, if $i_0 = 2$, then $F(\eta, \varphi) = F_2(\eta, \varphi) = \varphi_{x_1}\eta_{x_1} - \varphi_{x_2}\eta_{x_2}$.

2. There are several $\varepsilon(D_i, \varphi) = 1$, indicating that Q lies between several opposite currents. For example, $\varepsilon(D_1, \varphi) = \delta_{i,1} + \delta_{i,2}$, then let $F(\eta, \varphi) = rF_1(\eta, \varphi) + (1 - r)F_2(\eta, \varphi)$ in which $0 \leqslant r \leqslant 1$, $F_1(\eta, \varphi) = \varphi_{x_1}\eta_{x_1} - \varphi_{x_2}\eta_{x_2}$.

3. All $\varepsilon(D_i, \varphi) = 0$, indicating that Q is the center /134 or source of vorticity, and therefore $F(\eta, \varphi) = 0$. From this may be obtained the modified counter-wind scheme[7,22].

$$\left.\begin{aligned} &L_1(\eta, \varphi) = \eta_t + \theta\tau\eta_{tt} - F(\eta, \varphi) - \Delta^\nu(\eta + \sigma\tau\eta_t) - \chi\tau h^{-1}H^\nu(\eta) = f_1 \\ &L_2(\eta, \varphi) = f_2 \end{aligned}\right\} \quad (2.9)$$

III Error Estimation in Problems with Periodic Solution and the Generalized Stability

Let the difference scheme be $L_h[\eta(k)] = f(k)$ where $f(k)$ is the condition for solution determination. The error of f, will induce an error, $\bar{\eta}$, in η . Ordinarily, stability means that there exists an absolute constant M such that $\|\bar{\eta}\| \leqslant M\|\bar{f}\|$. However most non-linear schemes do not have such properties.

The author[7, 21, 22] suggested a generalized stability, namely that there exists positive numbers M, N and constant s independent of h, τ such that when $\leqslant Nh^{s}, k\tau \leqslant T \leqslant T_0(\|\tilde{f}\|)$, $\|\tilde{\eta}\| \leqslant M\|\tilde{f}\|$. The highest lower bound is called the index s of the generalized stability. Some explanations are offered below[21]:

1. For non-linear mechanical systems, generally only when $\|f\|$ satisfies certain conditicns will there exist a unique solution which is only stable against perturbations within certain range, e.g. the 3 dimensional Navier-Stokes Problem. But if $L_h 0 = 0, s \leqslant 0$, then when $\|f\| \leqslant N$, $\|\eta\| \leqslant M\|f\|$ and when $\|\tilde{f}\| \leqslant N$, $\|\tilde{\eta}\| \leqslant M\|\tilde{f}\|$. Clearly the value of s reflects exactly the properties stated above and therefore is suitable for non-linear systems.

2. The value of s may be used semi-quantitatively to reflect on the stability of round off errors. For example, the accuracy of a computer word is 2^{-l}, L_h in equation (2.7), $h=2^{-m}$, N_1 arithmetical computations are required for each η value calculated. Therefore, corresponding to $\|\tilde{f}\| \leqslant N_1 h^{-s} 2^{-l} \lambda^{-1}$, we should have $T_0 \leqslant \lambda N N_1^{-1} 2^{l-sm-\lambda m}$ to guarantee stability. Obviously the smaller s is, the more stable is the calculation, and the longer is the time of stability, T_0, and the more relaxed are the requirements on the computer word length and the step length.

3. For linear schemes, the generalized stability is equivalent to ordinary stability but they are not equivalent for non-linear schemes. Also if the formal approximate error of the scheme is $O(h^{s_0}), s_0 > k \geqslant 0$, then when $\xi \in c^k, s \leqslant s_0$, the k th order difference coefficient of η converges and is bounded.

4. In recent years, Weinberger et al.(see[10-12]) raised the problem of the optimization of scheme and they concentrated mostly on increasing the s_a of linear schemes. In this author's opinion, generally a non-linear scheme has weak discontinuities so s_a is not large. Hence the main direction of optimization is lowering the value of s. This will also improve the stability. Besides when s_a is small, we also have $s \leqslant s_a$, therefore is convergent. For detail, see [21, 22].

We shall estimate the upper bound of s below. $\tilde{\eta}, \tilde{\varphi}, \tilde{f}_i$ denote the computational error of η, φ, f_i. L, M, N, M_i are positive numbers,unrelated to h, τ, a, b are suitable positive numbers, m, ε are positive numbers yet to be determined.

$$m^* = \max\{2\sigma(2\sigma + \chi - 1)^{-1}, (2\theta + 1 + 12\chi\lambda\nu_1 + a)(1 + 2\theta)^{-1}\}$$
$$m^{**}(b) = [8\theta + 4a + 4 + 48\chi\lambda\nu_1 + 32\lambda\nu_1\sigma + 2b\lambda\nu_1\sigma]\{8\theta + 4 + 32\lambda\nu_1\sigma + 2b\lambda\nu_1\sigma - 16\lambda\nu_1 - b\lambda\nu_1 + 16\chi\lambda\nu_1 + b\chi\lambda\nu_1\}^{-1}$$

Condition $(\sigma, \lambda, \chi, \theta, b)$ shows that $\sigma_0 \geqslant (1-\chi)/2$, otherwise $\lambda < (8\theta + 4)\nu_1^{-1}(16 - 16\chi - 32\sigma + b - \chi b - 2b\sigma)^{-1}$. Condition $(\sigma, \lambda, \chi, \theta, b)_1$ shows that not only the conditions above hold, but also $2\delta > m^*$ when $\sigma_0 > (1-\chi)/2$, and $2\delta > m^{**}(b)$ when $\sigma_0 \leqslant (1-\chi)/2$.

The error equations of scheme (2.7) are

$$\left.\begin{aligned} \tilde{L}_1(\tilde{\eta}, \tilde{\varphi}) &= L_1(\tilde{\eta}, \tilde{\varphi}) - J(\tilde{\eta} + \delta\tau\tilde{\eta}_t, \varphi) - J(\eta + \delta\tau\eta_t, \tilde{\varphi}) = \tilde{f}_1 \\ \tilde{L}_2(\tilde{\eta}, \tilde{\varphi}) &= L_2(\tilde{\eta}, \tilde{\varphi}) = \tilde{f}_2 \end{aligned}\right\} \qquad (3.1)$$

Detailed calculation of $(2\tilde{\eta} + m\tau\tilde{\eta}_t, \tilde{L}_1(\tilde{\eta}, \tilde{\varphi}))$ gives from equation (1.1) - (1.8)

/135

$$B_{mnop}(\tilde{\eta}) + 2\|\tilde{\eta}\|_h^2 + \frac{1}{2}\theta m\tau^3\|\tilde{\eta}_{\bar{t}t}\|^2 - \frac{1}{2}\chi m\tau^3 D_+(\eta_t) - 2\tau\chi h^{-1}(\tilde{\eta}, H^*(\eta))$$
$$- \frac{1}{2}\chi m\tau^4 h^{-1}\sum_{l=1}^{3}(\nu_{\bar{s}_l}, \eta_t^2) + \sum_{l=1}^{4}\tilde{F}_l(\eta) - \sum_{l=0}^{5}\tilde{R}_l(\tilde{\eta}, \tilde{\varphi}) \qquad (3.2)$$

where

$$\tilde{F}_1 = -2B_{k_\Delta}^*(\nu, \bar{\eta}, \bar{\eta}_\alpha), \qquad \tilde{F}_2 = -m\tau B_{k_\Delta}^*(\nu, \bar{\eta}_t, \bar{\eta}_\alpha)$$
$$\tilde{F}_3 = -2\sigma\tau B_{k_\Delta}^*(\nu, \bar{\eta}, \bar{\eta}_{t\alpha}), \qquad \tilde{F}_4 = -m\tau^2\sigma B_{k_\Delta}^*(\nu, \bar{\eta}_t, \bar{\eta}_{t\alpha})$$

$$\tilde{E}_0 = \left(\frac{\sigma}{2} + \frac{m}{4}\right)\tau \sum_{j=1}^{3}(\nu_t, \bar{\eta}_{xj}^1 + \bar{\eta}_{tj}^2)$$

$$\tilde{E}_1 = (2\bar{\eta} + m\tau\bar{\eta}_t, J(\bar{\eta} + \delta\tau\eta_t, \bar{\varphi}) + \bar{\gamma}_1)$$
$$\tilde{E}_2 = (2\bar{\eta}, J(\bar{\eta} + \delta\tau\bar{\eta}_t, \bar{\varphi})), \qquad \tilde{E}_3 = (2\bar{\eta}, J(\bar{\eta} + \delta\tau\bar{\eta}_t, \varphi))$$
$$\tilde{E}_4 = m\tau(\bar{\eta}_t, J(\bar{\eta} + \delta\tau\bar{\eta}_t, \bar{\varphi})), \qquad \tilde{E}_5 = m\tau(\bar{\eta}_t, J(\bar{\eta} + \delta\tau\bar{\eta}_t, \varphi))$$

We can decompose $\tilde{E}_i = \tilde{E}_{i1} + \tilde{E}_{i2}$. . For example $\tilde{E}_{21} = 2(\bar{\eta}, J(\bar{\eta}, \bar{\varphi}))$, $\tilde{E}_{22} = 2\delta\tau(\bar{\eta}, J(\bar{\eta}_t, \bar{\varphi}))$, $\tilde{E}_{31} = 2(\bar{\eta}, J(\bar{\eta}, \varphi))$, $\tilde{E}_{32} = 2\delta\tau(\bar{\eta}, J(\bar{\eta}_t, \varphi))$ etc. If $\sigma_1 = \sigma_2$, then we get $\tilde{E}_{22} = \tilde{E}_{22}^* + \tilde{E}_{22}^{**}$ from equation (2.4), etc. Here

$$\tilde{E}_{21} = 2\sigma_1 B_{k_\Delta}^*(\bar{\eta}\bar{\varphi}_t, \bar{\eta}, 1) - 2\sigma_2 B_{k_\Delta}^*(\bar{\eta}_t\bar{\varphi}, \bar{\eta}, 1)$$
$$\tilde{E}_{22}^* = 2\delta\sigma_1\tau B_{k_\Delta}^*(\bar{\eta}\bar{\varphi}_t, \bar{\eta}_t, 1) + 2\delta\sigma_1\tau B_{k_\Delta}^*(\bar{\varphi}_t\bar{\eta}_t, \bar{\eta}, 1)$$
$$- 2\delta\sigma_2\tau B_{k_\Delta}^*(\bar{\eta}, \bar{\varphi}\bar{\eta}_{tt}, 1) - 2\delta\sigma_2\tau B_{k_\Delta}^*(\bar{\eta}_t, \bar{\varphi}\bar{\eta}_t, 1) \tag{3.3}$$
$$\tilde{E}_{22}^{**} = -2\delta\tau(\bar{\eta}_t, J(\bar{\eta}, \bar{\varphi}))$$
$$\tilde{E}_{31} = 2\sigma_1 B_{k_\Delta}^*(\bar{\eta}\varphi_t, \bar{\eta}, 1) - 2\sigma_2 B_{k_\Delta}^*(\bar{\eta}, \varphi\bar{\eta}_t, 1) \tag{3.4}$$

It can be proved that

$$|\theta|\tau^2\|\bar{\eta}_{tt}\|^2 \leq 2|\theta|\|\bar{\eta}_t\|^2 + 2|\theta|\|\bar{\eta}_t\|^2 \tag{3.5}$$

$$|2\chi\tau h^{-1}(\bar{\eta}, H^n(\eta))| \leq \frac{\chi}{2}\|\bar{\eta}\|_{1\infty}^2 + 12\chi\tau\lambda\nu_1\|\bar{\eta}_t\|^2 + \chi M_1\|\bar{\eta}\|^2 \tag{3.6}$$

$$\left|\frac{1}{2}\chi m\tau^2 h^{-1}\sum_{j=1}^{3}(\nu_{\theta j}, \bar{\eta}_t^2)\right| \leq \chi M_3\tau h\|\bar{\eta}_t\|^2 \tag{3.7}$$

We shall first estimate the periodic problem. To determine φ , let $\varphi(Q^*) = \text{const}$ at some point $Q^* \in R_{h_\Delta}$.

Theorem 1. Let scheme (2.7) satisfy conditions $(\sigma, \lambda, \chi, \theta, 0)$ and boundary conditions (A). Then 1. When $\|\bar{\gamma}_2\|^2$ and

$\rho(\bar{\eta}, \bar{f}_1, \bar{f}_2, 0, k)$ are not greater than Nh^{ν}, then for all $k\tau \leqslant T \leqslant T_0(\rho)$, we always have $\|\bar{\eta}(k)\|_{\infty,h}^2 \leqslant M e^{LT}\rho$. If when $\tau, h \to 0$, $\|\bar{f}_2\|^2 = O(\rho) = o(h^{\nu})$ then T_0 is arbitrary. Here, when $\nu_0 > 0$ or $\alpha_1 = \alpha_2$, $s \leqslant 1$. If $\nu_0 > 0$ and also $\alpha_1 = \alpha_2$, then $s \leqslant 0$. 2. If the conditions $(\sigma, \lambda, \chi, \theta, 0)$, are also satisfied, and $\alpha_1 = \alpha_2$, then for all $\bar{f}_2, \rho, T_0$, the above equation holds.

Proof: Equation (3.2) holds. From periodicity, $D_h(\bar{\eta}_i) = B_{R_h^*}(\nu, \bar{\varphi}, \bar{\varphi}_n) = \tilde{F}_i = 0$. Multiply the second equation of equation (3.1) by $\bar{\varphi}$ and find the inner product, from equation (1.5) and $\bar{\varphi}(Q^*) = 0$, it can be proved that there exists a constant m_0 related only to the diameter R_h such that

$$\|\bar{\varphi}\|^2 \leqslant m_0\|\bar{\varphi}\|_1^2 \leqslant 2m_0(\|\bar{\eta}\|^2 + \|\bar{f}_2\|^2) \tag{3.8}$$

From the Cauchy inequality and equation (3.8), we can get the estimation equation

$$|\tilde{E}_0| + |\tilde{E}_1| \leqslant M_3(\|\bar{\eta}\|^2 + \|\bar{\eta}\|^2 + \|\bar{f}_1\|^2 + \|\bar{f}_2\|^2 + \tau\|\bar{\eta}\|_1^2) \tag{3.9}$$ /136

If $\alpha_1 \neq \alpha_2$, but $\nu_0 > 0$, then from the Cauchy inequality, lemma 1 and equation (3.8), we can get as in [6]

$$|\tilde{E}_2| + |\tilde{E}_3| \leqslant \frac{a\tau}{4}\|\bar{\eta}_t\|^2 + \varepsilon\|\bar{\eta}\|_{1,h}^2 + \left(1 + \frac{1}{\varepsilon\nu_0}\right)M_4\|\bar{\eta}\|^2 \tag{3.10}$$

$$|\tilde{E}_3| + |\tilde{E}_4| \leqslant \frac{a\tau}{4}\|\bar{\eta}_t\|^2 + \varepsilon\|\bar{\eta}\|_{1,h}^2 + M_5h^{-2}\left(1 + \frac{1}{\varepsilon\nu_0}\right)\|\bar{\eta}\|^2(\|\bar{\eta}\|^2 + \|\bar{f}_2\|^2) \tag{3.11}$$

If $\alpha_1 = \alpha_2$, from the periodic condition (A) and equation (3.3), (3.4) we get $\tilde{E}_n = \tilde{E}_{n1}^* = \tilde{E}_M = 0$; ; from lemma 1 and equation (3.8) we also get

$$|\tilde{E}_M| \leqslant a\tau^2\|\eta_t\|_1^2 + M_6\|\bar{\eta}\|^2 \tag{3.12}$$

$$|\tilde{E}_{ij}^{n,*}| \leq \begin{cases} \frac{a\tau}{8}\|\tilde{\eta}_x\|^2 + M_7 a^{-1}\nu_0^{-1}\|\tilde{\eta}\|_{\nu_0}^2(\|\tilde{\eta}\|^2 + \|\tilde{f}_2\|^2), & \text{for } \nu_0 > 0 \\ \frac{a\tau}{8}\|\tilde{\eta}_x\|^2 + M_8 a^{-1}h^{-2}\|\tilde{\eta}\|^2(\|\tilde{\eta}\|^2 + \|\tilde{f}_2\|^2), & \text{for } \nu_0 = 0 \end{cases} \tag{3.13}$$

Similarly, we can estimate $|\tilde{E}_{21}|, |\tilde{E}_3|$. Substituting equation (3.5) - (3.13) into equation (3.2), we then obtain

$$\begin{aligned} B_{\alpha\alpha\tau\tau 0}(\tilde{\eta}) + \tau m\theta\|\tilde{\eta}_{\bar{t}}\|^2 + \tau(m\theta - \chi M_4 h - 12\chi\lambda\nu_1 - aM_{14})\|\tilde{\eta}_x\|^2 \\ + \|\tilde{\eta}\|_{\nu_0}^2 \leq \tilde{R}(\tilde{\eta}, 0) + f^*(\tilde{\eta}, 0)\|\tilde{\eta}\|_{\nu_0}^2 \end{aligned} \tag{3.14}$$

In this paper, let us denote

$$\begin{aligned} f^*(\tilde{\eta}, \tilde{g}) = & \cdots 1 + \frac{\chi}{2} + 2\delta + (1 - \operatorname{sign}|\alpha_1 - \alpha_2|)(M_9 h^{-1}\|\tilde{g}\|_{\hat{t}_\Delta}^2 \\ & + M_{10}\tau h\|\tilde{g}_x\|_{\hat{t}_\Delta}^2 + M_{11}\nu_0^{-1}\operatorname{sign}\nu_0(\|\tilde{\eta}\|^2 + \|\tilde{f}_2\|^2)) \\ \tilde{R}(\tilde{\eta}, \tilde{g}) = & [M_{12}h^{-2}(1 - \operatorname{sign}\nu_0 + \operatorname{sign}|\alpha_1 - \alpha_2|)\|\tilde{\eta}\|^2 + M_{13}h^{-1}(\|\tilde{g}\|_{\hat{t}_\Delta}^2 \\ & + \tau^2\|\tilde{g}_x\|_{\hat{t}_\Delta}^2)](\|\tilde{\eta}\|^2 + \|\tilde{f}_2\|^2) + M_{15}[\|\tilde{\eta}\|^2 + \|\tilde{\eta}\|^2 + \|\tilde{f}_1\|^2 \\ & + \|\tilde{f}_2\|^2 + h^{-1}\|\tilde{g}\|_{\hat{t}_\Delta}^2 + \tau h\|\tilde{g}_x\|_{\hat{t}_\Delta}^2] \end{aligned}$$

Let ϵ be suitably small, and multiply equation (3.14) by τ and find the sum over $j = 0, 1, 2, \cdots, k-1$, we then get

$$\begin{aligned} & \|\tilde{\eta}(k)\|_{\hat{\alpha}\hat{\alpha}\nu_0}^2 + \tau^2\rho_1\sum_{j=0}^{k-1}\|\tilde{\eta}_t(j)\|_{\nu_0}^2 + \tau^2\sum_{j=0}^{k-1}(\rho_2 + 2m\theta - \theta - 12\chi\lambda\nu_1 - aM_{14} \\ & - \chi M_3 h)\|\tilde{\eta}_x(j)\|^2 \leq \tau\sum_{j=0}^{k-1}[f^*(\tilde{\eta}(j), 0)\|\tilde{\eta}\|_{\nu_0}^2 + \tilde{R}(\tilde{\eta}(j), 0)] \\ & + |\theta|\|\tilde{\eta}(1)\|^2 + (1-\theta)\|\tilde{\eta}(0)\|^2 + \tau\left(\sigma + \frac{m}{2}\right)\|\tilde{\eta}(0)\|_{\nu_0}^2 \\ & + \frac{m|\theta|\tau^2}{2}\|\tilde{\eta}_t(0)\|^2 \end{aligned} \tag{3.15}$$

Let h be sufficiently small. If $\nu_0 > (1-\chi)/2$, then take $m > m_0^*$. Now coefficients of the 2nd and 3rd terms on the LHS of equation (3.15) are non-negative and may be neglected. And finally we only need to invoke lemma 4 and let

$w(k) = \|\tilde{\eta}(k)\|^2_{\delta_{n_1}}$, $v(k) = \|\tilde{\eta}(k)\|^2_{n_1}$, $n_1 = 0$. If $\alpha_1 = \alpha_2$ and $\nu_0 > 0$ then take $n_1 = 0$. Otherwise $n_1 = 2$. If $\sigma_0 \leqslant (1-\chi)/2$, then take $m > m^{**}(0)$. Because $\tau\|\tilde{\eta}_t\|^2_{n_1} \leqslant 8\lambda\nu_1\|\tilde{\eta}_t\|^2$ therefore the sum of the 2nd and 3rd terms on the LHS of equation (3.15) is non-negative. The proof below is similar to the above.

If further conditions $(\sigma, \lambda, \chi, \theta, 0)_1$ are satisfied, then we may take $m = 2\delta > m^{**}(0)$. From condition (A) and equation (2.5), $\sum_{i=2}^{\infty} \tilde{E}_i = 0$. After similar analysis we still get (3.14), but with $M_{11} = M_{12} = 0$. The rest of the proof may follow theorem 2 in [6].

Note 1. If $\nu_0 > 0$, then $s \leqslant 1$ for the explicit scheme. If $\alpha_1 = \alpha_2$, then in order to make the principle part of the non-linear error $(\tilde{\eta}, J(\tilde{\eta}, \tilde{\varphi})) = 0$, and thus $s \leqslant 0$. In this way, as long as ρ does not exceed a certain constant, the computation will be stable. At the same time, even if some singularities occur in $\frac{\partial \xi}{\partial t}$, etc. on the determinable long curve, as long as we still have the formal approximate error $\|\tilde{\eta}_i\| = o(1)$, the scheme still converges. If $\nu_0 = 0$, then as long as $\alpha_1 = \alpha_2$, then for sufficiently smooth solutions, $s_0 = 2 > s = 1$, the scheme will also converge. This explains why stability and the 2 conservation properties agree with one another. $\alpha_1 = \alpha_2$ is optional for both. /137

Note 2. For suitable χ, τ , the limit on λ may be relaxed. Suitable δ may eliminate non-linear error altogether so that the scheme may be used for the global solution calculation as well as being perfectly stable.

Note 3. If the modified counter-flow method is used, $s \leqslant 1$ can be proved as in [8, 22].

IV. Two Step Method in the Computation of Non-viscous flow

Two problems exist for non-viscous flow: 1. When $\theta = \delta = 0$, even if $\alpha_1 = \alpha_2$, $f_1 = 0$, we still have $\|\eta\|_1^2 = \tau\|\eta_1\|^2$. If the gradient is large, then the virtual growth of the energy is fairly rapid and computational overflow occurs. If an artificial viscosity term is used, the resolution in front of the wave will be lowered. Hence it is desirable to design a scheme that will automatically suppress this kind of growth. 2. In the explicit scheme of the last section, $s \leqslant 1$ but the true solution of the differential equation of non-viscous flow usually have weak discontinuities. In general $s_0 < 1$. Therefore we wish to design schemes with $s \leqslant 0$ to guarantee convergence.

Method I. Let η^* be the supplementary value.

$$\begin{aligned} &\text{Predictor} \quad \eta^* = \eta + \tau J^+(\eta, \varphi) \\ &\text{Corrector} \quad \eta = \frac{1}{2}(\eta + \eta^*) + \frac{\tau}{2} J^-(\eta^*, \varphi) \end{aligned} \tag{4.1}$$

If $\alpha_1 = 1$, this is equivalent to the Maccormack[13] method, but when $\alpha_1 = \alpha_2 = \frac{1}{2}$, $\|\eta_1\|^2 = \tau\|\eta_1\|^2 - \tau\|J^+(\eta, \varphi)\|^2$. Since equation (4.1) approximates equation (2.1), (when $\nu = f = 0$) therefore when $\|\eta_1\|^2$ is increased, generally $\|J^+(\eta, \varphi)\|^2$ also increases and therefore the virtual growth of the energy is automatically eliminated, giving a better result.

Method II. Split according to conservative type and non-conservative type. Equation

$$\eta^* = \eta + 2\tau J_1^+(\eta, \varphi), \quad \eta = \frac{1}{2}(\eta + \eta^*) + \tau J_1^-(\eta^*, \varphi) \tag{4.2}$$

It satisfies the energy relation

$$\|\eta_1\|^2 = \tau\|\eta_1\|^2 - 4\tau\|J_1^+(\eta, \varphi)\|^2$$

Computational experience shows that when J_1^+, J_1^- is used, the relationship between the order of J^+, J^- and the direction of wave propagation will markedly affect the computational accuracy. Therefore for systems with multi-directional wave propagation, we should use the average form, e.g. with J substituting for J+ etc.

Method III.

$$\eta^* = \eta + \beta\tau J(\eta, \varphi) + \tau^2 r\Delta\eta, \quad \eta = \eta + \tau J(\eta^*, \varphi) \tag{4.3}$$

If $\beta = \frac{1}{2}, \alpha_2 = 1, r = \frac{1}{4}h^2\tau^{-2}$, this is Lax-Wendroff scheme[4].

If $\beta = 1, \alpha_2 = 1, r = 0$, this is Matsuno scheme[14].

If $\beta = 1, \alpha_1 = \alpha_2 = \frac{1}{2}, r = 0$, then it is conservative and gives computational stability. Sometimes β may be taken to be slightly larger than 1.

Theorem 2. If in equation (4.3), $r = 0, \alpha_1 = \alpha_2 = 1/2, \beta > (3a + 1)/2, a > 0$, /138

$$\lambda < (2\beta - 3a - 1)^{\frac{1}{2}}[8\beta(3a + 1)\|\varphi\|_1]^{-1}a^{\frac{1}{2}}$$

then when $\|\bar{\eta}_2\|^2$ and $\rho(\bar{\eta}, \bar{\eta}_1, \bar{\eta}_2, 0, k)$ are not greater than N, we have $\|\bar{\eta}(k)\|^2 \leqslant Me^{LT}\rho$ for all $k\tau \leqslant T \leqslant T_0(\rho)$.

Proof. Let the computational error on the LHS be $\bar{\eta}_1, \bar{\eta}_1$. Then we have the following error equations:

$$\bar{\eta}_1 = J(\bar{\eta}, \varphi + \bar{\varphi}) + J(\eta, \bar{\varphi}) + \beta\tau J(J(\bar{\eta}, \varphi + \bar{\varphi}), \varphi + \bar{\varphi}) + \beta\tau J(J(\eta, \bar{\varphi}), \varphi + \bar{\varphi}) + \beta\tau J(J(\eta, \varphi), \bar{\varphi}) + \bar{\eta}_1$$

Multiplying the above equation with $2\bar{\eta} + \alpha_1\tau\bar{\eta}_1$ and calculating the inner product, we get

$$\|\bar{\eta}_{i+1}\|^2 + (m-1)\tau\|\bar{\eta}_i\|^2 + 2\beta\tau\|J(\bar{\eta}, \varphi+\bar{\varphi})\|^2 = \sum_{i=0}^{4}\tilde{G}_i$$

where

$$\begin{aligned}
\tilde{G}_0 &= (2\bar{\eta} + m\tau\bar{\eta}_i,\ J(\eta, \bar{\varphi}) + \beta\tau J(J(\eta, \varphi), \bar{\varphi}) + \bar{f}_1)\\
\tilde{G}_1 &= -2\beta\tau(J(\eta, \bar{\varphi}),\ J(\bar{\eta}, \varphi+\bar{\varphi}))\\
\tilde{G}_2 &= m\tau(\bar{\eta}_i,\ J(\bar{\eta}, \varphi+\bar{\varphi}))\\
\tilde{G}_3 &= m\tau^2\beta(\bar{\eta}_i,\ J(J(\bar{\eta}, \varphi+\bar{\varphi}), \varphi+\bar{\varphi}))\\
\tilde{G}_4 &= -\tau^2\beta(\bar{\eta}_i,\ J(J(\eta, \bar{\varphi}), \varphi+\bar{\varphi}))
\end{aligned}$$

We can prove

$$\begin{aligned}
|\tilde{G}_0| &\le M_{16}[\|\bar{\eta}\|^2 + \|\bar{\eta}_i\|^2 + \|\bar{\varphi}\|_1^2 + \|\bar{f}_1\|^2]\\
|\tilde{G}_1| &\le \tau^2\varepsilon\|J(\bar{\eta}, \varphi+\bar{\varphi})\|^2 + \frac{\beta^2}{\varepsilon}\|\bar{\varphi}\|_1^2\\
|\tilde{G}_2| &\le \tau(3a+1)\|J(\bar{\eta}, \varphi+\bar{\varphi})\|^2 + \frac{m^2\tau}{4(3a+1)}\|\bar{\eta}_i\|^2\\
|\tilde{G}_3| &\le a\tau\|\bar{\eta}_i\|^2 + 16\beta^2\tau^3 a^{-1}h^{-4}m^2\|J(\bar{\eta}, \varphi+\bar{\varphi})\|^2(\|\bar{\varphi}\|_1^2 + \|\varphi\|_1^2)\\
|\tilde{G}_4| &\le a\tau\|\bar{\eta}_i\|^2 + M_{17}\beta^2\tau^3 a^{-1}h^{-4}m^2(\|\bar{\varphi}\|^2 + \|\varphi\|^2)\|\bar{\varphi}\|_1^2
\end{aligned}$$

and hence

$$\begin{aligned}
&\|\bar{\eta}\|_1^2 + \tau(m-1-3a-\frac{1}{4}m^2(3a+1)^{-1})\|\bar{\eta}_i\|^2 + \tau(2\beta - \tau\beta - 3a - 1\\
&\quad - 16\lambda^2\beta^2 a^{-1}m^2\|\varphi\|_1^2 - 32\lambda^2 a^{-1}\beta^2 m^2 m_0\|\bar{f}_2\|^2)\|J(\bar{\eta}, \varphi+\bar{\varphi})\|^2\\
&\le 32\lambda^2 m^2 m_0\tau a^{-1}\beta^2\|\bar{\eta}\|^2\|J(\bar{\eta}, \varphi+\bar{\varphi})\|^2 + M_{18}[\|\bar{\eta}\|^2 + \|\bar{\eta}\|^2\\
&\quad + \|\bar{f}_1\|^2 + \|\bar{f}_2\|^2 + \tau^2 h^{-4}\|\bar{\eta}\|^4 + \tau^2 h^{-4}\|\bar{\eta}\|^2\|\bar{f}_2\|^2]
\end{aligned}$$

Now let $m = 6a + 2$, $\|\bar{f}_2\|^2$ be smaller than some constant, then the coefficient of the 2nd and 3rd terms of the RHS of the above equation are positive. Finally we use lemma 4 with $w(k) = \|\bar{\eta}(k)\|^2$.

Note 1. We can combine the weighted average conservative method with the Pycahob method, and the Kutler-Lomas-Warming

method as well as the method in [13].

Note 2. The method in this section is also suitable for shock wave computation. The author has applied it to calculate the double shock problem of the Burgers equation. The results show that the two step method can be used for many problems where one step methods cause overflow. The calculated result for $\alpha_1 = \alpha_2$ is the best. For system with multi-directional wave propagation, equation (4.3) is better than (4.1). The situation described by Theorem 2 is far better than the Lax-Wendroff scheme. For details, see [24].

Note 3. If equation (2.9) is used for non-viscous flow, then when $\tau \leqslant Nh$, $s \leqslant 1$[7] .

V. Effect of Boundary Value Error and Boundary Shape on Stability

/139

Assume that on Γ_1 , $\eta = g_1 \varphi - g_{1\tau} \tilde{g}_1$ represents the error in g_1. For convenience, let $\tilde{g}_0 = 0$. .

Theorem 3. Assume in equation (2.7) of the boundary value problem mentioned above, the conditions $(\sigma, \lambda, \chi, \theta, 1)$ are satisfied. In addition, if $\tilde{g}_1 \not\equiv 0$, then $\nu_* > 0$, σ^* is bounded, therefore 1. When $\|f_1\|'$, $h^{-1}\|\tilde{g}_1\|_4^1$ and $\rho(\eta, \tilde{\gamma}_1, \tilde{\gamma}_2, \tilde{g}_1 h^{-\frac{1}{2}}, k)$ not greater than Nh^{μ} , for all $k\tau \leqslant T \leqslant \gamma_0(\rho)$, we have $\|\eta(k)\|_{\omega_h} \leqslant M e^{LT} \rho$, where s is the same as in Theorem 1; 2. If $\alpha_1 = \alpha_2$ and the conditions $(\sigma, \lambda, \chi, \theta, 1)_4$ are also satisfied, then when $\|\tilde{g}_1\|_4^1 \leqslant Nh$ the above equation holds.

Proof. Multiply the second equation in equation (3.1) by $-\bar{\psi}$ and find the inner product. From equation (1.5), we get

$$\|\tilde{\varphi}_1\|_1^2 + \sum_{x_0^0} \tilde{\varphi}^2 \leqslant 2m_0^2 [\|\eta\|^2 + \|\tilde{\gamma}_2\|^2] \tag{5.1}$$

where

$$m_1 = \sup_{\tilde{\varphi}|\Gamma_h=0} \frac{\|\tilde{\varphi}\|^2}{\|\tilde{\varphi}\|_1^2}$$

Therefore the results similar to equation (3.1) - (3.13) all hold. [1)]

It can be proved that

$$-\frac{\chi m_1 \tau^2}{2} D_\nu(\eta_t) \geq \frac{\chi m \tau^2}{4}(1-\varepsilon)\sum_{K_h^0} \nu' \eta_t^2 - \chi\left(1+\frac{1}{\varepsilon}\right)\tau h M_{19}\|\tilde{g}_{1t}\|_{\Gamma_h}^2$$

$$F_1 \geq (1-\varepsilon)\sum_{K_h^0} \nu' \eta^2 - M_{20}(h^{-1}+h\varepsilon^{-1})\|\tilde{g}_1\|_{\Gamma_h}^2$$

$$F_2 \geq \frac{m\tau}{4}\left(\sum_{K_h^0} \nu' \eta^2\right)_t - \frac{m\tau^2}{4}\sum_{K_h^0} \nu' \eta_t^2 - \varepsilon\tau^2 \sum_{K_h^0} \nu' \eta_t^2 - \varepsilon a^* \sum_{K_h^0} \nu' \eta^2$$
$$- M_{21}[\tau h\|\tilde{g}_{1t}\|_{\Gamma_h}^2 + (\varepsilon h)^{-1}\|\tilde{g}_1\|_{\Gamma_h}^2 + \|\eta\|^2 + \|\eta\|^2]$$

$$F_3 \geq \frac{\sigma\tau}{2}\left[\sum_{K_h^0} \nu \eta^2\right]_t - \frac{\sigma\tau^2}{2}\sum_{K_h^0} \nu' \eta_t^2 - \varepsilon\tau^2 \sum_{K_h^0} \nu' \eta_t^2 - \varepsilon \sum_{K_h^0} \nu' \eta^2$$
$$- M_{22}[\tau h\|\tilde{g}_{1t}\|_{\Gamma_h}^2 + h^{-1}\varepsilon^{-1}\|\tilde{g}_1\|_{\Gamma_h}^2 + \|\eta\|^2 + \|\eta\|^2]$$

$$F_4 \geq \left(\frac{m\sigma}{2}-\varepsilon\right)\tau^2 \sum_{K_h^0} \nu' \eta_t^2 - M_{23}(1+h\varepsilon^{-1})\tau h\|\tilde{g}_{1t}\|_{\Gamma_h}^2$$

$$|2a_1 B_{K_h^0}(\eta\varphi_1, \eta, 1)| \leq M_{24}[\|\eta\|^2 + h^{-1}\|\tilde{g}_1\|_{\Gamma_h}^2]$$

$$|2a_3 B_{K_h^0}(\eta, \eta_1\varphi, 1)| \leq \varepsilon\|\eta\|_\nu^2 + \varepsilon \sum_{K_h^0} \nu' \eta^2 + a_3^2(\varepsilon h \nu_*)^{-1}\|\tilde{g}_1\|_{\Gamma_h}^2$$

(5.2)

Also because

$$\left|\sum_{K_h^0} hau\nu' w\right| \leq \frac{1}{2}\sum_{K_h^0} w^2 + \frac{1}{2}h^{-1}\|w\|^2\|\nu\|_{\Gamma_h}^2$$

Therefore

$$|2a_2 B_{K_h^0}(\eta\tilde{\varphi}_1, \eta, 1)| \leq \varepsilon \sum_{K_h^0} \nu' \eta^2 + \frac{a_2^2}{4\varepsilon\nu_* h}\|\tilde{\varphi}\|^2\|\tilde{g}_1\|_{\Gamma_h}^2$$

---

[1] When $\nu_* = 0$, an additional term $M_{25}\varepsilon^{-1}h^{-1}\|\tilde{g}_1\|_{\Gamma_h}^2(\|\eta\|^2 + \|\eta\|^2)$ is added to the RHS of equation (3.13). Similarly, equation (3.12) may be estimated.

$$|2\alpha_3 B R_h^*(\bar\eta, \bar\varphi\bar\eta_t, 1)| \leqslant \sum_{R_h^*} \bar\varphi^2 + \frac{\alpha_3^2}{4\nu_* h}\|\tilde g_1\|_{\tilde F_h}^2\|\bar\eta\|_{\nu_*}^2,$$

$$|2\delta\alpha_1\tau B_{R_h^*}(\bar\eta, \bar\varphi_1\bar\eta_t, 1)| \leqslant \varepsilon\tau^2\sum_{R_h^*}\nu'\bar\eta_t^2 + \frac{\delta^2\alpha_1^2}{\varepsilon\nu_* h}\|\tilde g_1\|_{\tilde F_h}^2\|\bar\varphi\|^2$$

$$|2\delta\alpha_1\tau B_{R_h^*}(\bar\eta_t, \bar\varphi_1\bar\eta, 1)| \leqslant \varepsilon\sum_{R_h^*}\nu'\bar\eta^2 + \frac{\delta^2\alpha_1^2}{\varepsilon\nu_*}\tau h\lambda\|\tilde g_{1t}\|_{\tilde F_h}^2\|\bar\varphi\|^2$$

$$|2\delta\alpha_1\tau B_{R_h^*}(\bar\eta, \bar\varphi\bar\eta_{1t}, 1)| \leqslant \sum_{R_h^*}\bar\varphi^2 + \frac{\delta^2\alpha_1^2\tau^2}{\nu_* h}\|\tilde g_1\|_{\tilde F_h}^2\sum_{R_h^*}\nu'\bar\eta_t^2$$

$$|2\delta\alpha_1\tau B_{R_h^*}(\bar\eta_t, \bar\varphi\bar\eta_t, 1)| \leqslant \sum_{R_h^*}\bar\varphi^2 + \frac{\delta^2\alpha_1^2\tau h\lambda}{\nu_*}\|\tilde g_{1t}\|_{\tilde F_h}^2\|\bar\eta\|_{\nu_*}^2.$$

Substituting equation (3.5) - (3.7), equation (3.9) - (3.13) and the equations above into equation (3.2), we obtain

$$b_{m+\alpha\beta}(\bar\eta) + \tau m\theta\|\bar\eta_t\|^2 + \tau(m\theta - 12\chi\lambda\nu_1 - hM_2\chi - aM_{14})\|\bar\eta_t\|^2 + \|\bar\eta\|_{\nu_*}^2 + \rho_3(\tilde g_1)\tau^2\sum_{R_h^*}\nu'\bar\eta_t^2 + (1 - 5\varepsilon - \varepsilon a^*)\sum_{R_h^*}\nu'\bar\eta^2 + \left(\frac{m}{4} + \frac{\sigma}{2}\right)\tau\left(\sum_{R_h^*}\nu'\bar\eta^2\right)_t \leqslant \tilde R(\bar\eta, \tilde g_1) + f^*(\bar\eta, \tilde g_1)\|\bar\eta\|_{\nu_*}^2,$$

where

$$\rho_3(\tilde g_1) = \frac{\chi m}{4} + \frac{m\sigma}{2} - \frac{\sigma}{2} - \frac{m}{4} - \frac{\chi m\varepsilon}{4} - 5\varepsilon - \varepsilon a^* - M_{25}h^{-1}\|\tilde g_1\|_{\tilde F_h}^2(1 - \operatorname{sign}|\alpha_1 - \alpha_2|)$$

Let ε be sufficiently small, and multiply the above equation with τ and also sum over $j=0, 1, 2, \cdots, k-1$. If $\sigma_0 > (1-\chi)/2$, then we take $m > m^*$. Now $\rho_1 \geqslant 0$, $\rho_2 + 2m\theta - \theta - 12\chi\lambda\nu_1 - aM_{14} - M_2h\chi \geqslant 0$ and if $h^{-1}\|\tilde g_1\|_{\tilde F_h}^2$ is sufficiently small, then $\rho_3(\tilde g_1) \geqslant 0$. If $\sigma_0 \leqslant (1-\chi)/2$ then we take $m > m^{**}(1)$. Since

$$\tau\sum_{R_h^*}\nu'\bar\eta_t^2 \leqslant \lambda\nu_1\|\bar\eta_t\|^2,$$

therefore

$$\tau\rho_1\|\bar\eta_t\|_{\nu_*}^2 + (\rho_2 + 2m\theta - \theta - 12\chi\lambda\nu_1 - aM_{14} - M_2h\chi)\|\bar\eta_t\|^2 + \tau\sum_{R_h^*}\rho_3(\tilde g_1)\nu'\bar\eta_t^2 \geqslant -h\|\tilde g_{1t}\|_{\tilde F_h}^2 \cdot \text{const}$$

The rest of the proof is similar to that used in Theorem 1.

Note 1. The effect of boundary value error on s is more pronounced. If $\tilde{g}_1 \equiv 0$, then when $\rho \leqslant Nh^{\mu}$, $\|\tilde{f}_2\|^2 \leqslant Nh^{\mu}$, the explicit scheme calculation is stable. If $\tilde{g} \not\equiv 0$, then we also need to have $\|\tilde{g}_1\|_{\Gamma_h}^2 \leqslant Nh^{\mu+1}$. Also if we take $\tilde{f}_1, \tilde{g}_1$ as the formal approximate error, then to guarantee convergence, we only require $\|\tilde{f}_1\|^2 = O(h^{\mu})$ but on the boundary, we need to require $\|\tilde{g}_1\|_{\Gamma_h}^2 = O(h^{\mu+1})$. But $\alpha_j = \omega_j$ still reaches the optimums as far as error control and the two conservation properties are concerned. It makes s decrease by 1, and when $\tilde{g}_1 = O(\sqrt{h})$, the scheme converges.

Note 2. If $\Gamma_h \neq 0$ then when $\nu_0 \equiv 0$, the explicit scheme computation of (2.7) still converges. If $\tilde{g}_1 \not\equiv 0$, then we require $\nu_0 > 0, \sigma^*$ to be bounded. In the language of numerical weather prediction, it means that there should be a smoothing process from the outside toward the inside, gradually decreasing in strength in the neighborhood of Γ_h. The calculation of Oliger and Sundstroun proved this[15]. /141

Note 3. By using methods similar to that in [8], it can be proved that if $\alpha_1 = \alpha_2 = 1/2$, $\nu_0 > 0$, scheme (2-8) has the same stability property as the implicit scheme (2.7), Therefore it is worthy of recommendation.

Note 4. If we calculate by using the modified counterflow method, it may be proved similar to [8] that when $\|f_1\|^2 = O(h^2)$, $\|\tilde{g}_1\|_{\Gamma_h}^2 = O(h^2)$, the calculation is stable and convergent. But this condition is too restrictive. The author proposes that in the vicinity of Γ_h, equation (2.9) should be used to be in agreement with the transport properties, and in the interior, equation (2.7) for $\alpha_1 = \alpha_2$ should be used to lower the s value. Shapiro and O'Brien, Williamson and

Browning had similar ideas.

Suitable boundary shape may lower the estimation of the upper bound of s.

Theorem 4. If the parameters in equation (2.7) satisfy the requirement of Theorem 3, R_h is a rectangle and there is no error in the boundary values, then even if $\delta = 0$, when $\|\vec{f}_2\|^2$ and $\rho(\vec{\eta}, \vec{f}_1, \vec{f}_2, 0, k)$ do not exceed Nh^{μ}, for all $k\tau \leqslant T \leqslant T_0(\rho)$, we have $\|\vec{\eta}(k)\|^2_{\omega_h} \leqslant Me^{LT}\rho$, where if $\alpha_1 = \alpha_2$ then $s \leqslant 0.5$, if $\nu_0 > 0$, then $s \leqslant 0$, and if $\alpha_1 = \alpha_2$ and $\nu_0 > 0$, then $s \leqslant -0.5$.

Proof. Similar to Theorem 3, but with $\tilde{g}_1 \equiv 0$. If $\alpha_1 = \alpha_2$ then $A = (\vec{\eta}, J(\vec{\eta}, \vec{\varphi})) = 0$, and if $\alpha_1 \neq \alpha_2$, then from lemma 2.3 and equation (5.1)

$$|A| \leqslant \frac{\varepsilon}{2}\|\vec{\eta}\|^2_{\omega_h} + \frac{3}{\varepsilon\nu_0}\|\vec{\eta}\|\|\vec{\eta}\|_1\|\vec{\varphi}\|_1\|\vec{\varphi}\|_2$$
$$\leqslant \frac{\varepsilon}{2}\|\vec{\eta}\|^2_{\omega_h} + \frac{6m_0'}{\varepsilon\nu_0^2}\|\vec{\eta}\|^2_{\omega_h}(\|\vec{\eta}\|^2 + \|\vec{f}_2\|^2)$$

Further

$$\tau|(\vec{\eta}_1, J(\vec{\eta}, \vec{\varphi}))| \leqslant \frac{\varepsilon\tau}{2}\|\vec{\eta}_1\|^2 + 12m_0'^2\varepsilon^{-1}\tau\|\vec{\eta}\|_1\|\vec{\eta}\|_2\|\vec{\varphi}\|_1\|\vec{\varphi}\|_2$$

When $\nu_0 > 0$, $\tau\|\vec{\eta}\|_1\|\vec{\eta}\|_2 \leqslant h\lambda M_2\nu_0^{-1}\|\vec{\eta}\|^2_{\omega_h}$, otherwise not greater than $h^{-1}M_2\|\vec{\eta}\|^2$. After the estimation by using the above method, we can finish the proof as in Theorem 3.

VI. Effect of the Type of Boundary Conditions

Assume that on Γ, $\frac{\partial\xi}{\partial n} + b\xi = g_1$ where $b \geqslant 0$. Its

difference approximation is

$$\eta_t(Q, k) + \frac{b}{2}[\eta(Q, k) + \eta(Q', k)] = g_2\left(\frac{Q + Q'}{2}, k\right), \quad Q \in R_h^* \qquad (6.1)$$

For convenience, let $\delta = \chi = 0, \nu = \text{const.}$, and the boundary shape be sufficiently regular.

Theorem 5. Assume that in scheme (2.7), and (6.1), $b = 0, \nu > 0$ and conditions $(\sigma, \lambda, 0, \theta, 0)$ are satisfied, then when $\|\tilde{\eta}_t\|^2$ and $\rho(\bar{\eta}, \tilde{\eta}_1, \tilde{\eta}_2, \tilde{g}_2, k)$ not greater than Nh^4, for all $k\tau \leq T \leq T_0(\rho)$, we have $\|\bar{\eta}(k)\|^2_{0\oplus\nu} \leq Me^{LT}\rho$.

Proof. Because

$$2B_{R_h^*}(\nu, u, v_t) = 2\nu h \sum_{R_h^*} u' v_t - \nu h^2 \sum_{R_h^*} u_t v_t$$

$$\|u\|^2_{\Gamma_h} \leq \text{const} \cdot (\|u\|^2 + \varepsilon\|u\|^2_1)^{1)}$$

Therefore /142

$$|\tilde{F}_1| \leq M_{17}(\|\bar{\eta}\|^2 + \|\tilde{g}_2\|^2_{\Gamma_h} + \varepsilon\|\bar{\eta}\|^2_{1\nu})$$

$$|\tilde{F}_2| \leq M_{18}(\tau^2\|\bar{\eta}_t\|^2 + \|\tilde{g}_2\|^2_{\Gamma_h} + \varepsilon\tau^2\|\bar{\eta}_t\|^2_{1\nu} + \tau^2\|\tilde{g}_{2t}\|^2_{\Gamma_h})$$

$$|\tilde{F}_3| \leq M_{19}(\|\bar{\eta}\|^2 + \tau^2\|\tilde{g}_{2t}\|^2_{\Gamma_h} + \varepsilon\|\bar{\eta}\|^2_{1\nu} + \|\tilde{g}_2\|^2_{\Gamma_h})$$

$$|\tilde{F}_4| \leq M_{20}\tau^2(\|\bar{\eta}_t\|^2 + \|\tilde{g}_{2t}\|^2_{\Gamma_h} + \varepsilon\|\bar{\eta}_t\|^2_{1\nu})$$

Substituting equation (3.5), (3.9) - (3.11) and the above equations into equation (3.2), we then get

$$\begin{aligned} &R_{\ldots}(\eta) + \tau m\theta\|\ldots\|^2 + \tau(m\theta - \varepsilon M_{14} - \tau M_{18} - \tau M_{20})\|\bar{\eta}_t\|^2 \\ &+ (2 - 2\varepsilon - M_{17}\varepsilon - M_{18}\varepsilon - M_{19}\varepsilon)\|\bar{\eta}\|^2_{1\nu} - \varepsilon\tau^2\|\bar{\eta}_t\|^2_{1\nu}(M_{18} \\ &+ M_{20}) \leq M_{21}(\|\bar{\eta}\|^2 + \|\bar{\eta}\|^2 + h^{-2}(\|\bar{\eta}\|^2 + \|\tilde{\eta}_2\|^2)\|\bar{\eta}\|^2 \\ &+ \|\tilde{g}_2\|^2_{\Gamma_h} + \tau^2\|\tilde{g}_{2t}\|^2_{\Gamma_h}) \end{aligned}$$

The rest of the proof follows similar lines as Theorem 3.

---

[1] For proof, see another paper of mine. From this get

$$|2B_{R_h^*}(\nu, u, v_t)| \leq \text{const} \cdot (\|u\|^2 + \|v_t\|^2_{\Gamma_h} + \|u_t\|^2_{\Gamma_h} + \varepsilon\|u\|^2_{1\nu}).$$

Finally in lemma 4, let $w(k) = \|\bar{\eta}(k)\|^2_{\mathring{\Theta}_h}$, $n_1 = 2, n_2 = 0$.

Theorem 6. If in schemes (2.7), and (6.1), $b > 0, \nu > 0$, and conditions $(\sigma, \lambda, 0, \theta, 0)$ are satisfied, then when $\|\bar{f}_h\|^2$ and $\rho(\bar{\eta}, \bar{f}_1, \bar{f}_2, \bar{g}_2, k)$ not greater than Nh^4, for all $k\tau \leqslant T \leqslant T_0(\rho)$ we have

$$\|\bar{\eta}(k)\|^2_{\mathring{\Theta}_h} \leqslant M e^{LT} \rho$$

Proof. Since on Γ_h

$$\bar{\eta}_{\bar{x}} = -\frac{b}{2}(\bar{\eta} + \bar{\eta}') + \bar{g}_2, \quad 2\eta\eta_t = (\eta^2)_t - \tau(\eta_t)^2$$

therefore

$$F_1 \leqslant \frac{b\nu h}{4}(1 - \varepsilon) \sum_{\kappa_h^*} (\bar{\eta} + \bar{\eta}')^2 - M_{10}\|\bar{g}_2\|^2_{\mathring{\Theta}_h}$$

$$F_2 \geqslant \frac{bm\tau\nu h}{8} \sum_{\kappa_h^*} (\bar{\eta} + \bar{\eta}')_t^2 - \frac{b\nu m\tau^2 h}{8}(1 + \varepsilon) \sum_{\kappa_h^*} (\bar{\eta}_t + \bar{\eta}_t')^2 - M_{11}\|\bar{g}_2\|^2_{\mathring{\Theta}_h}$$

$$F_3 \geqslant \frac{b\nu\sigma\tau h}{4} \sum_{\kappa_h^*} (\bar{\eta} + \bar{\eta}')_t^2 - \frac{\nu\sigma\tau^2 hb}{4}(1 + \varepsilon) \sum_{\kappa_h^*} (\bar{\eta}_t + \bar{\eta}_t')^2 - M_{12}\tau^2\|\bar{g}_{2t}\|^2_{\mathring{\Theta}_h}$$

$$F_4 \geqslant \frac{b\nu\sigma m\tau^2 h}{4}(1 - \varepsilon) \sum_{\kappa_h^*} (\bar{\eta}_t + \bar{\eta}_t')^2 - M_{13}\tau^2\|\bar{g}_{2t}\|^2_{\mathring{\Theta}_h}$$

Substituting equation (3.5), (3.9) - (3.11) and the above equations into equation (3.2), we get

$$B_{n+\sigma}(\bar{\eta}) + \varepsilon m\theta\|\bar{\eta}_t\|^2 + \tau(m\theta - M_{14}\varepsilon)\|\bar{\eta}_t\|^2 + 2(1 - \varepsilon)\|\bar{\eta}\|^2_+$$
$$+ \frac{b\nu h}{2}(1 - \varepsilon) \sum_{\kappa_h^*} (\bar{\eta} + \bar{\eta}')^2 + \frac{b\nu\tau h}{4}\left(\sigma + \frac{m}{2}\right) \sum_{\kappa_h^*} (\bar{\eta} + \bar{\eta}')_t^2$$
$$+ \frac{b\nu\tau^2 h}{4}\left(\sigma m - \sigma - \frac{m}{2} - \sigma m\varepsilon - \sigma\varepsilon - \frac{m}{2}\varepsilon\right) \cdot \sum_{\kappa_h^*} (\bar{\eta}_t + \bar{\eta}_t')^2$$
$$\leqslant M_{15}(\|\bar{\eta}\|^2 + \|\bar{\eta}\|^2 + h^{-2}\|\bar{\eta}\|^2(\|\bar{\eta}\|^2 + \|\bar{f}_h\|^2) + \|\bar{g}_2\|^2_{\mathring{\Theta}_h} + \tau^2\|\bar{g}_{2t}\|^2_{\mathring{\Theta}_h})$$

The rest of the proof is similar to that for Theorem 5.

Note 1. From Theorems 5 and 6, if $\bar{g}_2 = 0$ then when

$\|\tilde{\gamma}_h\|^2, \rho \leqslant Nh^2$ the computation is stable. If $\tilde{g}_i \not\equiv 0$ then we need to require $\|\tilde{g}_i\|_h \leqslant Nh^2$ in order to guarantee stability. If we treat $\tilde{\gamma}_h, \tilde{g}_i$ as formal approximate error, then when $\|\tilde{\gamma}_h\|^2 = O(h^2), \|\tilde{g}_i\|_h = O(h^2)$, schemes (2.7), (6.1) converge. This can be achieved by suitably choosing Γ_h.

Note 2. The following externally imposed boundary conditions are often used in numerical weather forecast: /143

$$\eta(Q') = \eta(Q), \quad Q \in R_h^*$$

or

$$\eta(Q') = 2\eta(Q) - \eta(Q^{**}), \quad Q \in R_h^*$$

where $Q^{**} \in R_h - R_h^*$ and distance h from Q. These 2 conditions may be considered as conditions (6.1), with accuracy O(1) and O(h) respectively. Theorem 5 cannot guarantee the convergence in long term calculations. The calculation of Platzman and Mastuno proved this. For reference, see [14].

Note 3. The method in this paper may be used to prove the suitability of many boundary treatment methods in aerodynamics. For example, $\psi = g_0, \frac{\partial \psi}{\partial n} = g_1, g_2$ is often given on Γ according to the famous Thom method, i.e. [1]

$$\eta(Q') = \xi(Q') = -2(\psi(Q') - \psi(Q))h^{-1} + O(h)$$
$$= -2h^{-1}g_1\left(\frac{Q+Q'}{2}\right) + O(h)$$

This is equivalent to the boundary value conditions of the first kind of η with error $O(h)$. From Theorem 3, this method of treatment will lead to a convergent result.

Note 4. We may also adopt various boundary conditions of ψ. For example, $\varphi_0 = g_4$ with error $\tilde{g}_4$. Let us construct

a function $\tilde{G}_4$ such that $\tilde{G}_4|_{\Gamma_4} = \tilde{g}_4$. Also let $\tilde{\varphi} = \tilde{G}_4 + \bar{\varphi}$, then $\Delta\bar{\varphi} = \tilde{\eta}_1 - \Delta\tilde{G}_4 + \tilde{\eta}$, $\bar{\varphi}_4|_{\Gamma_4} = 0$. Hence we can prove that there exists a constant m_0'' only dependent on the diameter of the region such that

$$\|\bar{\varphi}\|_1^2 \leqslant \|\bar{\varphi}\|_{m_0''}^2 \leqslant 2m_0''\|\tilde{G}_4\|_1^2 + 8m_0''^2(\|\tilde{\eta}\|^2 + \|\tilde{\eta}_1\|^2 + \|\Delta\tilde{G}_4\|^2)$$

By substituting this estimation equation into the earlier theorems as $\|\bar{\varphi}\|_1^2$, we will get the corresponding result.

Note 5. By combining the various methods in this paper, we can prove the convergence of the computational methods of many practical problems, for instance the example of a wind tunnel calculation on page 140 in Reference [1]. From symmetry, we know $\psi = \xi = 0$. on the center line Γ_1 of the wind tunnel. On the surface Γ_3 of the object, we know $\psi = 0$ from fixed wall boundary. ξ is treated by using Thom's condition. At Γ_4 upstream, $u = u_0, v = v_0$. Therefore ψ is known, and $\xi = \text{const}$ by Daugherty's method. On the fixed walls of the wind tunnel, since $v = 0$, ψ is known. ξ is calculated by Mueller's method. At Γ_2 downstream,

$$\frac{\partial\xi}{\partial n} = \frac{\partial\psi}{\partial n} = 0.$$

This method of treating boundary conditions will lead to a stable and convergent numerical result.

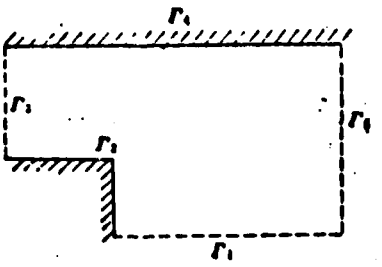

Figure 1

VII. Dynamic Relaxation Method for Steady Flow /144

Consider the problem of steady flow

$$\left.\begin{aligned} &\frac{\partial \xi}{\partial x_1}\frac{\partial \psi}{\partial x_2}-\frac{\partial \xi}{\partial x_2}\frac{\partial \psi}{\partial x_1}+\frac{\partial}{\partial x_1}\left(\nu\frac{\partial \xi}{\partial x_1}\right)+\frac{\partial}{\partial x_2}\left(\nu\frac{\partial \xi}{\partial x_2}\right)=-f_1\\ &\nabla^2\psi-\xi=f_2 \end{aligned}\right\} \tag{7.1}$$

For convenience, assume $f_2\equiv 0, \nu=\text{const}$, , zero boundary value and R a rectangle. In [1, 3, 5] many computational methods are introduced but there is no proof whether solution exists for the corresponding difference scheme or whether the solution is bounded for all h. In this paper the following scheme is given

$$J(\eta,\varphi)+\nu\Delta\eta=-f_1,\quad \Delta\varphi=\eta \tag{7.2}$$

Assume H is the Hilbert space formed by the net functions that satisfy the zero boundary value condition under the inner product

$$[w,v]=\frac{1}{2}[(w_{x_1},v_{x_1})+(w_{x_2},v_{x_2})]+\frac{1}{2}\sum_{x\in\delta}wv$$

The norm is denoted by $\|\cdot\|_H$. Obviously for arbitrary $w\in H$, (w,f_1) is a linear functional in H. Hence there exists $F\in H$ such that $[F,w]=(w,f_1)$ and $|(w,f_1)|\leqslant\|F\|_H\|w\|_H$.

Theorem 7. In (7.2), if $\alpha_1=\alpha_2$, , and $\|F\|_H$ is uniformly bounded for h, then for all h, there exists at least one solution of equation (7.2) uniformly bounded for h.

Proof. Multiply equation (7.2) by $w\in H$ and find the inner product. From equation (1.4), we get

$$-\nu[\eta,w]+(w,J(\eta,\varphi))=-(f_1,w)$$

But for fixed η and φ, $(w, J(\eta, \varphi))$ is also a linear functional in H. Hence there exists $A\eta \in H$ such that $[A\eta, w] = (w, J(\eta, \varphi))$. Therefore the solution of equation (7.2) is equivalent to the solution of the following non-linear operator equation:

$$\eta - \frac{1}{\nu}(A\eta + F) = 0 \tag{7.3}$$

Assume that there is a sequence $\eta^{(n)}$, $\Delta\varphi^{(n)} = \eta^{(n)}$. When $n \to \infty$, $\|\eta^{(n)} - \eta\|_H \to 0$. Hence when n is sufficiently large, $\|\eta^{(n)}\|_H$, $\|\varphi^{(n)}\|_H$ is uniformly bounded. Denote $s^{(m,n)} = [A\eta^{(m)} - A\eta^{(n)}, w]$ then from equation (2.4) and lemma 2, we have

$$|s^{(m,n)}| \leqslant |(\eta^{(m)} - \eta^{(n)}, J(w, \varphi^{(m)})| + |\eta^{(n)}, J(w, \varphi^{(m)} - \varphi^{(n)}))| \leqslant M_w \|\eta^{(m)} - \eta^{(n)}\|_H \|w\|_H$$

Take $w = A\eta^{(m)} - A\eta^{(n)}$, then $\|A(\eta^{(m)} - \eta^{(n)})\|_H \leqslant M_w \|\eta^{(m)} - \eta^{(n)}\|$, i.e. A is a continuous operator and M_w is independent of h. Now from Browder's fixed point theorem, we only need to prove that the equation

$$\eta - \lambda(A\eta + F) = 0 \tag{7.4}$$

is bounded for the set of all possible solutions of $\lambda \in [0, 1/\nu]$. Multiply the 2 sides of (7.4) with $\eta^{(\lambda)}$ and find the inner product in H, we have

$$\|\eta^{(\lambda)}\|_H^2 \leqslant \lambda \|\eta^{(\lambda)}\|_H \|F\|_H \leqslant \frac{1}{\nu} \|\eta^{(\lambda)}\|_H \|F\|_H.$$

Theorem 8. If $2\sqrt{2}\,(m_0')^{1/2}\|f_1\| \leqslant \nu^2$, $a_1 = a_2$ then the solution of (7.2) is unique.

Proof. Assume η, φ and η', φ' are both solutions. $\eta' = \eta + \tilde{\eta}, \varphi' = \varphi + \tilde{\varphi}$, then

$$\nu\Delta\bar{\eta} + J(\bar{\eta}, \varphi + \bar{\varphi}) + J(\eta, \bar{\varphi}) = 0, \quad \Delta\bar{\varphi} = \bar{\eta}$$

Multiply the first equation with η on both sides and find its inner product. We also notice that

$$\|\eta\|^{\frac{1}{2}}\|\eta\|_1^{\frac{1}{2}} \leqslant m_0^{\frac{1}{2}}\|f_1\|\nu^{-1}, \ \|\bar{\varphi}\|_2^2 \leqslant \|\Delta\bar{\varphi}\|^2 \leqslant \|\bar{\eta}\|^2 \leqslant m_0'\|\bar{\eta}\|_1^2,$$

therefore

$$\nu\|\bar{\eta}\|_H^2 \leqslant 2\sqrt{2}\,\|\bar{\eta}\|_1\|\eta\|^{\frac{1}{4}}\|\eta\|_1^{\frac{1}{4}}\|\bar{\varphi}\|_1^{\frac{1}{4}}\|\bar{\varphi}\|_2^{\frac{1}{4}}$$

$$\leqslant 2\sqrt{2}\,m_0^{\frac{1}{4}}\|\eta\|^{\frac{1}{4}}\|\eta\|_1^{\frac{1}{4}}\|\bar{\eta}\|_1\|\bar{\varphi}\|_2 \leqslant 2\sqrt{2}\,\nu^{-1}\|f_1\|m_0^{\frac{1}{2}}\|\bar{\eta}\|_H^2 \qquad /145$$

Theorem 9. Assume the ith equation in (7.2) has error $\bar{f}_i$, and the corresponding η has error $\bar{\eta}$, then under the same conditions as in Theorem 8, $\|\bar{\eta}\|^2 \leqslant M_{37}[\|\bar{f}_1\|^2 + \|\bar{f}_2\|^2]$.

Theorem 10. Under the conditions of Theorem 8, the following iteration process converges at least as a geometric series where τ is the relaxation factor and n the number of iteration:

$$\left.\begin{aligned}\eta^{(n+1)} &= \eta^{(n)} + \tau[\nu\Delta\eta^{(n+1)} + J(\eta^{(n+1)}, \varphi^{(n)}) + f_1] \\ \Delta\varphi^{(n+1)} &= \eta^{(n+1)} + f_2\end{aligned}\right\} \qquad (7.5)$$

The two theorems above may be proved similar to [8]. If $\alpha_1 = 1$, equation (7.5) is then the N-S method in [5]. Apparantly this method of calculation and proof is more complicated. In recent years, Davis, Greenspan and Hodgkings have all tried to calculate equation (7.1) with non-steady state method. For reference, see [1, 17, 18]. They call this the dynamic relaxation method. But since equation (7.1) is a nonlinear problem, thus violating the simple relationship between the steady flow iteration process and the final state of nonsteady flow as pointed out by Frankel. Therefore very few theoretical results have been derived. This author examined

this problem from another angle, and first proved that generalized solutions exist for both equation (2.1) and (7.1) under very weak conditions. He also proved that if the generalized Reynold number $Re^* = 2\sqrt{2}\, m_0^{*\frac{1}{2}} \nu^{-1} \|f_1\|_{L_1} < 1$ then equation (7.1)'s solution is unique, where

$$\|\xi\|_{L_1}^2 = \iint_R \xi^2 dx_1 dx_2, \quad \|\xi\|_{L_2^{-1}}^2 = \iint_R \left[\left(\frac{\partial \xi}{\partial x_1}\right)^2 + \left(\frac{\partial \xi}{\partial x_2}\right)^2\right] dx_1 dx_2$$

$$\|\xi\|_{W_2^1}^2 = \|\xi\|_{L_2}^2 + \|\xi\|_{L_2^{-1}}^2, \quad \|\xi\|_{L_2^{-2}}^2 = \sum_{i=1}^{2} \left\| \frac{\partial \xi}{\partial x_i} \right\|_{L_2^{-1}}^2$$

H^* is the closure of the infinitely smooth, finite subset functions under $\|\cdot\|_{W_2^1}$, and

$$m_0^* = \sup_{\xi \in H^*} \frac{\|\xi\|_{L_2}^2}{\|\xi\|_{L_2^{-1}}^2}$$

We denote $\alpha = 2\nu(m_0^*)^{-1}(1 - Re^*)$.

Theorem 11. If ξ is the solution of (7.1), $\xi(t)$ is the solution of (2.1), both with zero boundary values, $\xi(t) = \xi(t) - \xi$, then when $Re^* < 1$.

$$\|\xi(t)\|_{L_2}^2 \leq e^{-\alpha t} \|\xi(0)\|_{L_2}^2$$

Proof:

$$\left.\begin{aligned} &\frac{\partial \xi}{\partial t} - \frac{\partial \xi}{\partial x_1}\frac{\partial(\psi + \tilde{\psi})}{\partial x_2} + \frac{\partial \xi}{\partial x_2}\frac{\partial(\psi + \tilde{\psi})}{\partial x_1} - \nu \nabla^2 \xi = \frac{\partial \xi}{\partial x_1}\frac{\partial \tilde{\psi}}{\partial x_2} - \frac{\partial \xi}{\partial x_2}\frac{\partial \tilde{\psi}}{\partial x_1} \\ &\nabla^2 \tilde{\psi} = \xi \end{aligned}\right\} \quad (7.6)$$

Multiply both sides of the first equation by 2ξ and find its inner product. We get

$$\begin{aligned} \frac{d\|\xi\|_{L_2}^2}{dt} + 2\nu\|\xi\|_{L_2^{-1}}^2 &\leq 2\|\xi\|_{L_2^{-1}} \left(\left\| \xi \frac{\partial \tilde{\psi}}{\partial x_1} \right\| + \left\| \xi \frac{\partial \tilde{\psi}}{\partial x_2} \right\| \right) \\ &\leq 2\|\xi\|_{L_2^{-1}}^{\frac{1}{2}} \|\xi\|_{L_2}^{\frac{1}{2}} \|\xi\|_{L_2^{-1}} \|\tilde{\psi}\|_{L_2^{-1}}^{\frac{1}{2}} \|\tilde{\psi}\|_{L_2^{-2}}^{\frac{1}{2}} \\ &\leq 2m_0^* \nu^{-1} \|f_1\|_{L_2} \|\xi\|_{L_2^{-1}} \|\tilde{\psi}\|_{L_2^{-2}} \end{aligned}$$

From an inequality in § 1, Chapter 1 of Reference [9], $\|\psi\|_{L_2}^2 \leqslant \|\nabla^2\psi\|_{L_2}^2 \leqslant \|\xi\|_{L_2}^2 \leqslant m_0^*\|\xi\|_{L_2}^2$, therefore

$$\frac{d}{dt}\|\xi\|_{L_2}^2 + \frac{2\nu}{m_0^*}(1 - \mathrm{Re}^*)\|\xi\|_{L_2}^2 \leqslant 0$$

Since a systematic result has been established for non-steady flow in our paper, we may conclude by using Theorem 11 as follows: /146

1. For any $-\varepsilon > 0$, we may choose $T_0 = \frac{2}{\alpha}\left|\log\frac{\varepsilon}{2\|\xi(0)\|_{L_2}}\right|$ so that when $t \geqslant T_0$, $\|\xi - \xi(t)\| \leqslant \frac{\varepsilon}{2}$. Further if we assume that the approximate value $\eta(t)$ of $\xi(t)$ is calculated by using any one of the schemes in § 2, then we can prove that if conditions in Theorem 1 - 6 are satisfied and $\rho \leqslant M_1 h^{2\mu_0}$, then when $h \leqslant \sqrt[2\mu_0]{\frac{\varepsilon^2 e^{-LT_0}}{4MM_1}}$ 时

$$\|\eta(T_0) - \xi(T_0)\| < \varepsilon/2$$

so that $\|\eta(T_0) - \xi\| < \varepsilon$, i.e. when the above process is considered as an iteration process with relaxation factor τ, the process is convergent.

2. Iterative convergence depends on many factors. If v is too small or $\|f_1\|_{L_2}$ too big, the conditions of Theorem 11 will both be violated so that the total iterative procedure may not converge. If h is too big, then no matter how big is T_0, $\eta(t)$ will not converge in $\xi(t)$. If τ is too small, the amount of work will be increased; if τ it too big, then the conditions of Theorems 1 - 6 will be violated and the iterative process may not converge. From the process of proof we see that the iterative convergence is related to initial iterative error, boundary shape, type of boundary condition as well as to boundary value error. This agrees with the experience described by Greenspan[17], Roach[1], etc.

3. The amount of work may also be estimated. For example if equation (2.7) is used in the calculation, the total number of iterations is about

$$K_0 = \frac{T}{\lambda h^2} = O\left[\frac{2}{\lambda a}\left|\log\frac{\varepsilon}{2\|\xi(0)\|_{L_1}}\right|\left(\frac{4MM_1}{\varepsilon^2}\right)^{\frac{1}{\nu\alpha}}\left\|\frac{\varepsilon}{2\|\xi(0)\|_{L_1}}\right|^{\frac{2L}{\alpha\nu}}\right]$$

Apparently when ν, ε are large, K_0 is small. When $\|f_1\|, \|\xi(0)\|_{L_1}$ or M, M_1 (gradient correspondong to the solution) are large, K_0 is large.

When Theorem 11 is applied to local district numerical weather forecast, it shows that if v is fairly large and the η , φ values on the boundary are fixed, then when $h \to 0, \tau \to 0$, $\eta(t) \to \xi(t)$ and when T_0 is sufficiently large, $\xi(t)$ approaches ξ, i.e. the forecast value rapidly transits toward equilibrium. Therefore the sponge boundary conditions in [20] should be used. For more detailed proof and application of some of the results in this paper, see Reference [21-24].

References

[1] Roach, P. J., Computational Fluid Dynamics, Hermosa Publishers (1972).
[2] Ames, W. F., *SIAM Review*, 15 (1973), 524—552.
[3] Dorodnichn, A. A., Proc. of 3rd International Conference, on Numerical Method in Mechanics(July 3—7, 1972), 1—11.
[4] Richotmyer, R D., Morton, K. W., Difference Methods for Initial Value Problems, 2nd. Interscience Publishers, New York (1967).
[5] Greenspan, D., Discrete Numerical Methods in Physics and Engineering, Academic Press, New York (1974).
[6] Guo Benyi, Acta Mathematica Sinica 17 (1974), 242-258.
[7] Guo Benyu, Acta Mathematica Sinica 21 (1976), 127=131.
[8] Kuo Pen-yu (郭本瑜), *Scientia Sinica* (1977), 287—304.
[9] Ладыженская, О. А., Математические вопросы динамики вязкой несжимаемой жидкости, ФИЗМАТ ГИЗ, (1961).
[10] Weinberger, H. F., *SIAM. J., Numer. Anal.*, 9 (1972), 182—198.
[11] Miccnelli, C. A. and Miranker, W. F., *SIAM. J., Numer. Anal.*, 10 (1973), 983—1009.
[12] Birkhoff, G. and Gulati, S., *SIAM J., Numer. Anal.*, 11 (1974), 700—728.
[13] MaccorMack, R. W. and Balduin, B. S., AIAA, (1975).
[14] Haltiner, G. J., Numerical Weather Prediction, John Wiley (1971).
[15] Shapiro, M. A. and o'Brien, J. J., *J. Appl. Meteor.*, 9 (1970), 345—349
[16] Williamson, D. L. and Browning, G. L., *J. Appl. Meteor.*, 13 (1974), 8—16.
[17] Greenspan, D., *J. Computer*, 12 (1969), 88—93.
[18] Hodgkins, W. R., *Numer. Math.*, 9 (1967), 446—451.
[19] Heywood, J. G., *Archive for Rational Mechanics and Analysis*, 37 (1970), 48—60.
[20] Perkey, P. J. and Kreitsberg, C. W., *M. W. R.*, 104 (1976), 744—755.

/147

[21] Guo Benyu Atmospheric Science 2 (1978) 103-114.
[22] Guo Benyu Journal of Applied Mathematics 1 (1978) 181-192.
[23] Guo Benyu Journal of Science 23 (1978) 424-429.
[24] Guo Benyu Computational Mathematics 4 (1978) 79-90.

Abstract

There are five important subjects in the theory of difference methods: 1. construction of scheme; 2. Stability of scheme; 3. Computation of flow without viscous term; 4. Interference of boundary conditions; 5. Solution of steady flow. A lot of work has been done in this field[1-7], but no systematic theory has been developed.

In this paper, systematic results are provided with particular reference to two-dimensional vorticity equation. Two classes of schemes are constructed based on conservation and transport property. A new concept concerning generalized stability and optimization of nonlinear scheme is introduced. The index s to generalized stability for periodic problem is estimated, which shows the relationship of stability and conservation. Two-level schemes are given to decrease the index s. The influences of bound shape, boundary conditions and their errors are fully discussed. Finally the existence of the solution of steady flow is proved and a dynamic relaxation method is proposed. Several examples are given, showing that the methods suggested here are useful both for numerical weather prediction, and in the field of aerodynamics and other subjects.

ON THE KERNEL FUNCTION COLLOCATION METHOD IN STEADY SUBSONIC FLOW FOR WING WITH CONTROL SURFACES*

Chen Jing Song
Nanjing Aeronautic Institute

ABSTRACT

In this paper the forms of the lift distribution function for wings with control surfaces in steady subsonic flow are analyzed. Methods for treating kernel singularities of linear integral equations and singularities of the lift distribution function are discussed and the numerical solution to the integral equation is given. The method in this paper may be used to calculate the lift distribution of the wing by itself or of the wing with partial or full control surfaces on both the leading and trailing edges. The numerical values agree well with experimental data and have the same accuracy as those given by other theories. As compared with the vortex-lattice method, the computational storage requirement for our method is smaller and the computational time is less. The numerical computation may be carried on smaller computers.

I. FOREWORD

At present, the numerical methods to solve the lift surface linear integral equation are categorized into two kinds: The vortex lattice method and the kernel function method. The advantage of the vortex lattice method is that it is not necessary to assume a priori the form of the lift distribution function, and hence, in principle, there does not exist any difficulty to compute problems involving partial control surfaces. However, to achieve a certain computational accuracy, the number of vortex lattices should be

*Received February 11, 1974

large and this will certainly result in a higher order for the linear algebraic equations of the coefficients. The advantage of the kernel function method is that it requires very few collocation points and, therefore, the order of the equations to solve for the undetermined coefficients is low. Its difficulty lies in the fact that the lift distribution function with matching boundary conditions and edge conditions must be chosen a priori. Reference [3] made use of a method of approximate expansion to study the pressure amplitude characteristics of the leading and trailing edges as well as the corner when the control surfaces oscillate harmonically and obtained the "form for the control surface lift distribution", thus making it possible to solve the control surface problem with the kernel function method.

There are two methods of treatment when the kernel function method is used to solve the control surface problem. One of these is to substitute directly into the integral equation the control surface lift distribution as obtained by the approximate expansion method to find the downstream velocity induced at the collocation points on the wing (including the control surfaces). The equivalent downstream velocity is then obtained by subtracting this induced velocity from the actual downstream velocity at this collocation point. In this way, we may solve for the lift distribution that satisfies this equivalent downstream velocity with the kernel function method, while regarding the wing with control surface as one without. Then by super-imposing this distribution to the control surface lift distribution mentioned above, the lift distribution on a wing with harmonically oscillating control surfaces is obtained. This kind of method is called the equivalent downstream velocity kernel function collocation method.[4-6]

To obtain a stable solution for the equivalent downstream velocity kernel function collocation method, the number of collocation points should be somewhat large. It is also necessary to select an expansion factor for the control surface lift distribution, but it

is difficult to make it satisfy the edge condition of a flat plane while keeping the second order derivative of the lateral load continuous. Shortly after the completion of the work in this paper in August of 1973, we saw that some progress had been done along this direction in [6]. Some of the problems are solved but the region of integration has to be subdivided into many smaller regions during numerical integration. The technique of using just a few collocation points and integration points as in the control surface kernel function method cannot be used. In this paper we use the control surface kernel function method to determine the lift distribution of the control surfaces. Limited by space, only the results for the steady flow will be presented in this paper.

II. FUNDAMENTL EQUATIONS

The fundamental equation of steady subsonic lift surface theory is

$$w(x, y) = \frac{1}{4\rho U_\infty \pi} \iint_{S_w} \Delta P(\xi, \eta) K(x - \xi, y - \eta, M_\infty) d\xi d\eta \qquad (1)$$

where w is the downstream distribution function over the wing; ρ and U_∞ are the incoming flow density and velocity; ΔP is the lift distribution function of the wing and is a constant; $K = -\frac{1}{(y-\eta)^2} \cdot \left[1 + \frac{x-\xi}{\sqrt{(x-\xi)^2 + \beta^2(y-\eta)^2}}\right]$ is the kernel function; M_∞ is the incoming flow Mach number, $\beta = \sqrt{1 - M_\infty^2}$.

According to Figure 1, by transforming the coordinates in Equation (1) and making use of the conditions that ΔP is zero at both tips of the wing, we obtain

$$W(\bar{x}, \bar{y}) = \frac{1}{S_0} \int_{-1}^{1} \frac{\partial}{\partial \eta} \left\{ \int_{-1}^{1} \Delta P(\xi, \eta) \left[1 + \frac{\bar{x} - \xi}{R}\right] b(\eta) d\xi \right\} \frac{d\eta}{\bar{y} - \eta} \qquad (2)$$

where $W = 4\pi\rho U_\infty w(\bar{x}, \bar{y})$, $R = \sqrt{(\bar{x} - \xi)^2 + \beta^2(\bar{y} - \eta)^2}$, . In the above, the dimensionless coordinates are respectively

$$\left.\begin{aligned} \bar{x}, \bar{y}; \xi, \eta &= \left(\frac{x}{b_0}\right), \left(\frac{y}{b_0}\right); \left(\frac{\xi}{b_0}\right), \left(\frac{\eta}{b_0}\right) \\ x, y; \xi, \eta &= \left(\frac{x - x_m(y)}{b(y)}\right), \left(\frac{y}{S_0}\right); \left(\frac{\xi - \xi_m(\eta)}{b(\eta)}\right), \left(\frac{\eta}{S_0}\right) \end{aligned}\right\} \qquad (2a)$$

physical plane

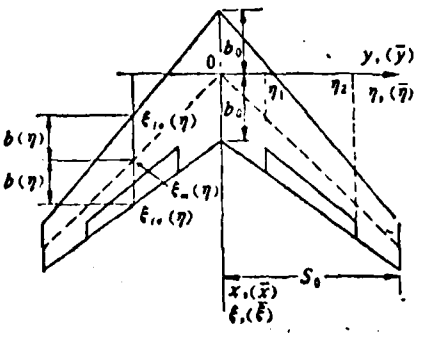

transformation plane

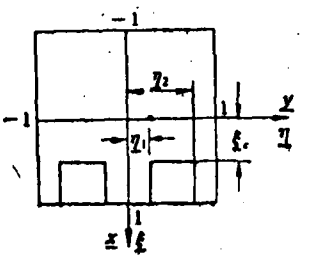

Figure 1. The physical plane and transformation plane of the wing.

The meanings of the other symbols are shown in Figure 1.

To obtain a convergent solution with suitable accuracy, to reduce the required machine memory and to shorten the computational time, before solving the integral Equation (2), we must first select a suitable lift distribution function, find the best

positions of the integration point, the downstream point and use a stable and effective numerical integration technique.

III. SELECTION OF THE FORM OF LIFT DISTRIBUTION FUNCTION

According to linear theory, the lift distribution may be divided into two parts: the normal part ΔP_R as produced by the incident angle when your angle is zero and the subsidiary part ΔP_{CSR} as produced by the zero angle when the incident angle is 0.

$$\Delta P(\xi, \eta) = \Delta P_R(\xi, \eta) + \Delta P_{CSR}(\xi, \eta) \tag{3}$$

The function ΔP_R is required to be continuous on the wing with an inverse square root singularity at the leading edge of the wing, to satisfy the Kutta-Joukowski condition at the trailing edge and to vanish at the side edges with a square root form. Hence, the tangent direction of ΔP_R may be chosen to be the first few terms of the accurate thin wing solution and the lateral direction to be the elliptic distribution solution of a (long, narrow slender body) wing [7,8].

$$\Delta P_R(\xi, \eta) = \frac{4\rho U_\infty^2}{b(\eta)} S_0 \sqrt{1-\eta^2}\left[g_0(\eta)\sqrt{\frac{1-\xi}{1+\xi}} + g_1(\eta)(1-\xi^2)^{1/2} + g_2(\eta)(1-\xi^2)^{1/2}\xi + \cdots\right] \tag{4}$$

where

$$g_n(\eta) = a_{n0}U_0(\eta) + a_{n1}U_1(\eta) + a_{n2}U_2(\eta) + \cdots (n = 0, 1, \cdots, N) \tag{5}$$

(N + 1) is the number of terms along the tangent direction of the lift distribution function; $U_m(\eta)$ is the Chebyshev polynomial of second kind;(m = 0, 1, ..., M) is the number of terms in the lateral direction; a_{nm} are the undetermined coefficients to be found by satisfying the boundary conditions. It is easy to see from Equation (4) that ΔP_R does have the proper edge properties.

The zero incident angle slender body lift distribution [9] of the partial control surface (with axis of rotation along the leading edge) is

$$\Delta p_{csR}(\xi) = \Delta p_{cs}(\xi) + \Delta p_R(\xi)$$
$$\propto \left[\ln \left| \frac{1 - \xi\xi_c + \sqrt{1-\xi^2}\sqrt{1-\xi_c^2}}{\xi - \xi_c} \right| + \sqrt{\frac{1-\xi}{1+\xi}} \cos^{-1}\xi_c \right]$$

where Δp_{cs} is called the control surface lift distribution function. It is proportional to the logarithmic term. Δp_R is called the normal lift distribution function. Similarly, the zero incident angle lift distribution function of the wing with partial control surface consists also of two parts. The form of ΔP_R is similar to Equation (4). ΔP_{cs} may be expressed according to the form supplied by [3] in conjunction with the logarithmic term solution of the wing type discussed above as [7]

$$\Delta P_{cs}(\xi, \eta) = \frac{4\rho U_\infty^2}{b(\eta)} S_0 \sqrt{1-\eta^2} [g_0(\eta) + g_1(\eta)(1+\xi) + \cdots] \varphi_{cs}(\xi, \eta) \tag{6a}$$

where

$$\varphi_{cs}(\xi, \eta) = \sum_{n=1}^{ICS} \ln \left| \frac{\{[1 - \xi\xi_{cn} + (1-\xi^2)^{1/2}(1-\xi_{cn}^2)^{1/2}]^2 + E_n^2\}^{1/2} - E_n}{[(\xi - \xi_{cn})^2 + E_n^2]^{1/2} - E_n} \right|$$
$$E_n = \begin{cases} \beta^2(\eta - \eta_{1n})(\eta_{2n} - \eta), & \eta \geq 0 \\ -\beta^2(\eta + \eta_{1n})(\eta_{2n} + \eta), & \eta < 0 \end{cases} \tag{6b}$$

Summarizing the above discussions, the lift distribution function of the wing with partial control surface at zero angle is

$$\Delta P_{csR}(\xi, \eta) = \frac{4\rho U_\infty^2}{b(\eta)} S_0 \sqrt{1-\eta^2} \{ [g_0(\eta) + g_1(\eta)(1+\xi) + \cdots] \varphi_{cs}(\xi, \eta) \tag{7}$$
$$+ [g_{JC}(\eta) \left(\frac{1-\xi}{1+\xi}\right)^{1/2} + g_{(JC+1)}(\eta)(1-\xi^2)^{1/2} + g_{(JC+2)}(\eta)(1-\xi^2)^{1/2}\xi + \cdots] \}$$

In Equations (6a) to (7), ICS is the number of control surfaces that move together in the right half of the wing; for the meaning of ξ_{cn}, η_{1n} and η_{2n}, see Figure 2; JC is the number of tangential terms of ΔP_{cs}. For the case of leading and trailing edge control surfaces that rotate together, JC=2. Otherwise JC=1. For the tangential terms of ΔP_R, at least two terms should be

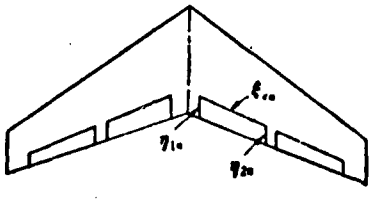

Figure 2. Diagram showing the control surfaces on the wing

taken. It is not difficult to verify from Equation (6) that $\Delta\Gamma_{cs}$ has the property as pointed out in [3]: namely, that it is zero at the leading and trailing edges of the wing, finite at the side edge of the control surface and continuous on the wing surface outside the control surfaces.

IV. THE BEST POSITIONS OF DOWNSTREAM POINT AND INTEGRATION POINT AND TECHNIQUE OF NUMERICAL INTEGRATION

It can be proved that to minimize the difference between the approximate values of the low speed thin wing lift and the total lift and their respective exact values, the tangential downstream point and the lateral downstream chord should be respectively [10]

$$x_i = -\cos\left(\frac{2i\pi}{2I+1}\right) \quad (i = 1, 2, \cdots, I) \tag{8}$$

$$y_r = \cos\left(\frac{r\pi}{2R'+1}\right) \quad (r = 1, 2, \cdots, R') \tag{9}$$

where I is the number of downstream points of each chord; R' is the number of downstream chords of the right half wing. The best ratio of R'/I may be obtained following [7] for various wing shapes and M_∞.

From the functional forms as shown in Equations (4) and (7), we can use the Gauss-Mehler quadrature with $\sqrt{(1-\xi)/(1+\xi)}$ as weight to maximize the accuracy of the tangential numerical integration of Equation (2)

$$\int_{-1}^{1}\sqrt{\frac{1-\xi}{1+\xi}}\,f(\xi)\,d\xi \approx \sum_{i=1}^{J} H_i f(\xi_i) \tag{10a}$$

where J is the number of integration points of each chord. The integration point and weighting coefficient are respectively

$$\left.\begin{aligned} \xi_i &= -\cos\left[\frac{2i-1}{2J+1}\pi\right] \quad (i = 1, 2, \cdots, J) \\ H_i &= \frac{2\pi}{2J+1}(1-\xi_i) \end{aligned}\right\} \tag{10b}$$

If $f(\xi)$ is a polynomial with order less than $(2J - 1)$, then Equation (10a) is the exact value.

Substituting Equation (4) (or Equation (7)) into Equation (2), we may obtain the general form for the lateral integral

$$I(\gamma) = \int_{-1}^{1} \frac{\partial}{\partial \eta}[\sqrt{1-\eta^2}\, G(\gamma, \eta)] \frac{1}{\gamma - \eta} d\eta \tag{11}$$

$G(\underline{y},\underline{\eta})$ is the tangential integral of Equation (2). We may assume that it is an analytic function of $\underline{\eta}$. Since it is impossible to numerically integrate Equation (11) directly, we first expand $G(\underline{y},\underline{\eta})$ into a Taylor series and then integrate termwise to get

$$I(\gamma) \approx -\sum_{s=1}^{S} H_s \left\{ \frac{(1-\eta_s^2)[G(\gamma, \eta_s) - G(\gamma, \gamma)]}{(\gamma - \eta_s)^2} + \frac{(1-\gamma^2)G'(\gamma, \gamma)}{\gamma - \eta_s} \right\} + \pi G(\gamma, \gamma) \tag{12a}$$

where S is the number of integration chords of the whole wing; $\underline{\eta}_s$ and H_s are respectively the integration point and weighting coefficient of the Gauss-Mehler quadrature Equation (11) with $1/\sqrt{1-\eta^2}$ as weight.

$$\left.\begin{aligned} \eta_s &= -\cos\left(\frac{2s-1}{2S}\pi\right) \quad (s = 1, 2, \cdots, S) \\ H_s &= \pi/S \end{aligned}\right\} \tag{12b}$$

It will be proved below that Equation (12a) may be greatly simplified by appropriately collocating the positions of the downstream chords and the integration chord.

Since the positions of the integration chords mentioned above $\underline{\eta}_1, \ldots, \underline{\eta}_1$ are the zero points of $T_S(\underline{\eta})$, therefore

$$T_S(\eta) = 2^{S-1} \prod_{s=1}^{S} (\eta - \eta_s) \tag{13a}$$

The logarithmic derivative of (13a) is

$$T_S'(\eta)/T_S(\eta) = \sum_{s=1}^{S} \frac{1}{\eta - \eta_s} \tag{13b}$$

If we let $2R' + 1 = S$, i.e., take $\underline{y}_r$ as the zero point of $T_S'(\underline{\eta})$ then $\underline{\eta}_s$ and $\underline{y}_r$ become crossed. Also from Equation (13b)

$$\sum_{i=1}^{s} \frac{1}{\chi_r - \eta_i} = 0 \tag{13c}$$

Hence, Equation (12a) may be simplified as

$$I(\chi_r) \approx -\frac{\pi}{S} \sum_{i=1}^{s} \frac{(1-\eta_i)^2 G(\chi_r, \eta_i)}{(\chi_r - \eta_i)^2} + \pi G(\chi_r, \chi_r)\left[1 + \frac{1}{S} \sum_{i=1}^{s} \frac{1-\eta_i^2}{(\chi_r - \eta_i)^2}\right] \tag{13d}$$

We shall prove below that the square bracket portion of Equation (13d) is equal to S. Change the variable $\underline{\eta}$ in Equation (13b) to $\underline{y}$ and differentiate. We then get

$$\sum_{i=1}^{s} \frac{1}{(\chi - \eta_i)^2} = [T_s'(\chi)/T_s(\chi)]^2 - T_s''(\chi)/T_s(\chi) \tag{13e}$$

According to the property of Chebyshev polynomial,

$$(1-\chi^2)T_s''(\chi) - \chi T_s'(\chi) + S^2 T_s(\chi) = 0 \tag{13f}$$

Therefore, we get from Equations (13e,f) and the fact that $\underline{y}_r'$ is the zero point of $T_S'(\underline{y})$:

$$\sum_{i=1}^{s} \frac{1}{(\chi_r - \eta_i)^2} = \frac{S^2}{(1-\chi_r^2)} \tag{13g}$$

Since $(1-\eta_i^2) = (1-\chi_r^2) + 2\chi_r(\chi_r - \eta_i) - (\chi_r - \eta_i)^2$, therefore,

$$\sum_{i=1}^{s} \frac{1-\eta_i^2}{(\chi_r - \eta_i)^2} = (1-\chi_r^2) \sum_{i=1}^{s} \frac{1}{(\chi_r - \eta_i)^2} + 2\chi_r \sum_{i=1}^{s} \frac{1}{\chi_r - \eta_i} - \sum_{i=1}^{s} 1 \tag{13h}$$

It may finally be proved from Equations (13c,g,h) that the square bracket portion of Equation (13d) is S. Hence, the numerical integral (12a) is finally simplified [10] as

$$I(\chi_r) = \int_{-1}^{1} \frac{\partial}{\partial \eta}[\sqrt{1-\eta^2}\, G(\chi_r, \eta)] \frac{1}{\chi_r - \eta} d\eta \approx -\frac{\pi}{S} \sum_{i=1}^{s} \frac{(1-\eta_i^2) G(\chi_r, \eta_i)}{(\chi_r - \eta_i)^2} + \pi S G(\chi_r, \chi_r) \tag{14}$$

If $G(\underline{y},\underline{\eta})$ is the (2S - 1) or lower order polynomial of $\underline{\eta}$, then Equation (14) is the exact value.

V. INTEGRATION OF THE INTEGRAL EQUATION AND ITS SOLUTION

1. Case of angle $\alpha \neq 0$ and yaw angle $\delta = 0$.

Substituting the lift distribution function Equation (4) into the integration formula (2) and applying Equation (14), we get

$$\frac{W_K(\bar{x}, \bar{y}_r)}{4\rho U_\infty^2} = -\frac{\pi}{S} \sum_{r=1}^{s} \frac{(1-\eta_r^2) G_K(\chi_r, \eta_r)}{(\chi_r - \eta_r)^2} + \pi S G_K(\chi_r, \chi_r) \tag{15}$$

where

$$G_K(\chi, \eta) = \int_{-1}^{1} \phi_K(\xi, \eta) \left[1 + \frac{\bar{x} - \xi}{R}\right] d\xi \tag{16}$$

$$\phi_K(\xi, \eta) = [g_0(\eta) + g_1(\eta)(1+\xi) + g_2(\eta)\xi(1+\xi) + \cdots] \sqrt{\frac{1-\xi}{1+\xi}} \tag{17}$$

In Equation (16), the function being integrated has a jump discontinuity at $\xi = \bar{x}$ along $\eta = \bar{y}$. Because of this, Equation (16) is rewritten as

$$G_K(\chi, \eta) = \int_{-1}^{1} [\phi_K(\xi, \eta) - \phi_K(\xi, \chi)] \left[1 + \frac{\bar{x} - \xi}{R}\right] d\xi + \int_{-1}^{1} \phi_K(\xi, \chi) \left[1 + \frac{\bar{x} - \xi}{R}\right] d\xi \tag{18}$$

Thus, the singularity of the integrand in the first integral may be found by using the quadrature Equation (10). Jump discontinuity still exists in the second integrand which is difficult to integrate analytically. Hence, we expand the analytic function $\phi_K(\xi, \chi)$ into a Taylor series:

$$\phi_K(\xi, \chi) = \phi_K(x, \chi) + (\xi - x)\phi_{Kx}(x, \chi) + \cdots \tag{19}$$

while from Equation (2a) and Figure 1, it can be shown that

$$(\xi - x) = [b_0/b(\eta)](\xi - \bar{x}) + [b_0/b(\eta)][\bar{x} - \xi_{LE}(\eta)] - (1 + x) \tag{20}$$

Substituting Equations (19) and (20) into Equation (18), the second integral can then be integrated analytically. If only the first two terms of the series are taken, then after some algebra, the result of integration is

$$G_K(\chi, \eta) = \frac{2\pi}{2J+1} \sum_{j=1}^{J} [g_0(\eta)(1-\xi_j) + g_1(\eta)(1-\xi_j^2) + \cdots] \cdot \left[1 + \frac{\bar{x}_i - \xi_j}{R_{ij}}\right] + \sum_{p=0}^{1} \phi_{Kp}(x_i, \chi)\psi_{Kp}(\bar{x}_i, \bar{y}, \eta) \quad (21)$$

where

$$\phi_{K0}(x, \chi) = \left(\frac{1-x}{1+x}\right)^{1/2} [g_0(\chi) + g_1(\chi)(1+x) + g_2(\chi)x(1+x) + \cdots] \quad (22)$$

$$\phi_{K1}(x, \chi) = \frac{\partial}{\partial x}[\phi_{K0}(x, \chi)] \quad (23)$$

$$\psi_{K0}(\bar{x}, \bar{y}, \eta) = \left\{H_0(\bar{x}, \bar{y}, \eta) - \frac{2\pi}{2J+1} \sum_{j=1}^{J} (1-\xi_j^2)^{1/2}\left[1 + \frac{\bar{x} - \xi_j}{R_j}\right]\right\} \quad (24)$$

$$\psi_{K1}(\bar{x}, \bar{y}, \eta) = \left[\frac{b_0(\bar{x} - \xi_{1e}(\eta))}{b(\eta)} - (1+x)\right]\psi_{K0}(\bar{x}, \bar{y}, \eta) + \frac{b_0}{b(\eta)}\left\{H_1(\bar{x}, \bar{y}, \eta) - \frac{2\pi}{2J+1} \sum_{j=1}^{J} (1-\xi_j^2)^{1/2}(\bar{x} - \xi_j)\left[1 + \frac{\bar{x} - \xi_j}{R_j}\right]\right\} \quad (25)$$

$$H_0(\bar{x}, \bar{y}, \eta) = 2 + \frac{b_0}{b(\eta)}\{[(\bar{x} - \xi_{1e})^2 + \beta^2(\bar{y} - \eta)^2]^{1/2} - [(\xi_{1e} - \bar{x})^2 + \beta^2(\bar{y} - \eta)^2]^{1/2}\} \quad (26)$$

$$H_1(\bar{x}, \bar{y}, \eta) = -\frac{1}{2}\frac{b_0}{b(\eta)}\left\{(\bar{x} - \xi_{1e})^2 - (\xi_{1e} - \bar{x})^2 + (\bar{x} - \xi_{1e})[(\bar{x} - \xi_{1e})^2 + \beta^2(\bar{y} - \eta)^2]^{1/2} + (\xi_{1e} - \bar{x})[(\xi_{1e} - \bar{x})^2 + \beta^2(\bar{y} - \eta)^2]^{1/2} - \beta^2(\bar{y} - \eta)^2 \ln\left|\frac{[(\bar{x} - \xi_{1e})^2 + \beta^2(\bar{y} - \eta)^2]^{1/2} + (\bar{x} - \xi_{1e})}{[(\xi_{1e} - \bar{x})^2 + \beta^2(\bar{y} - \eta)^2]^{1/2} - (\xi_{1e} - \bar{x})}\right|\right\} \quad (27)$$

$$G_K(\chi, \chi) = \lim_{\eta \to \chi} G_K(\chi, \eta) \quad (28)$$

Substituting Equations (21) and (28) into Equation (15), the downstream distribution expression for $\alpha \neq 0$, $\delta = 0$ is

$$\frac{W_K(\bar{x}_i, \bar{y}_i)}{4\rho U_\infty^2} = \frac{-2\pi^2}{S(2J+1)} \sum_{i=1}^{s} \sum_{l=1}^{s} \frac{(1-\eta_l^2)}{(\chi_r - \eta_l)^2} [g_0(\eta_l)(1-\xi_j) + g_1(\eta_l)(1-\xi_j^2) + \cdots] \cdot \left[1 + \frac{\bar{x}_i - \xi_j}{\sqrt{(\bar{x}_i - \xi_j)^2 + \beta^2(\bar{y}_i - \eta_l)^2}}\right] + \frac{2\pi^2 S}{2J+1} \sum_{j=1}^{J} [g_0(\chi_r)(1-\xi_j) + g_1(\chi_r)(1-\xi_j^2) + \cdots] \cdot \left[1 + \frac{x_i - \xi_j}{|x_i - \xi_j|}\right] - \frac{\pi}{S} \sum_{i=1}^{s} \frac{(1-\eta_i^2)}{(\chi_r - \eta_i)^2} \Psi_{GK}(x_i, \chi_r, \eta_i) + \pi S \Psi_{GK}(x_i, \chi_r, \chi_r) \quad (29)$$

The last two terms in the above equation are the correction terms that appear when the jump discontinuity in the integrand is eliminated. In the above,

$$\Psi_{GK}(x, \gamma, \eta) = \sum_{p=0}^{1} \phi_{Kp}(x, \gamma) \cdot \psi_{Kp}(\bar{x}, \bar{y}, \eta) \tag{30}$$

2. The case of $\alpha = 0$, $\delta \neq 0$.

From the simultaneous Equations (2), (7) and (14), we obtain

$$\frac{W_{CSK}(\bar{x}, \bar{y}_r)}{4\rho U_\infty^2} = -\frac{\pi}{S} \sum_{r=1}^{s} \frac{(1-\eta_r^2) G_{CSK}(\gamma_r, \eta_r)}{(\gamma_r - \eta_r)^2} + \pi S G_{CSK}(\gamma_r, \gamma_r) \tag{31}$$

where

$$G_{CSK}(\gamma, \eta) = G_{CSK1}(\gamma, \eta) + G_{CSK2}(\gamma, \eta) \tag{32}$$

$$G_{CSK1} = \int_{-1}^{1} [g_0(\eta) + g_1(\eta)(1+\xi) + \cdots] \varphi_{CS}(\xi, \eta) \left[1 + \frac{\bar{x} - \xi}{R}\right] d\xi \tag{33a}$$

$$G_{CSK2} = \int_{-1}^{1} [g_{JC}(\eta) + g_{(JC+1)}(\eta)(1+\xi) + \cdots] \sqrt{\frac{1-\xi}{1+\xi}} \left[1 + \frac{\bar{x} - \xi}{R}\right] d\xi \tag{34a}$$

Equation (34a) is similar to Equation (16). The result of integration is

$$G_{CSK2}(\gamma, \eta) = \frac{2\pi}{2J+1} \sum_{j=1}^{J} [g_{JC}(\eta)(1-\xi_j) + g_{(JC+1)}(\eta)(1-\xi_j^2) + \cdots] \cdot \left[1 + \frac{\bar{x}_i - \xi_j}{R_{ij}}\right] + \sum_{p=0}^{1}{}' \phi_{Kp}(\bar{x}_i, \gamma) \psi_{Kp}(\bar{x}_i, \bar{y}, \eta) \tag{34b}$$

Except for the jump discontinuity at $\eta = \bar{y}$, $\xi = \bar{x}$, the integrand in Equation (33a) has a logarithmic discontinuity at the leading edge of the control surface. The method of eliminating the former is as described in the above section. The logarithmic singularity is eliminated by a method similar to that used to eliminate the jump discontinuity. To make the correction term that changes the integral from singular to non-singular consistent along the lateral direction, the lateral part of the non-singular term is also corrected. The final result of Equation (33a) after this treatment is

$$G_{CSKi}(\chi,\eta)=\frac{2\pi}{2J+1}\sum_{j=1}^{J}\left[g_0(\eta)(1-\xi_j)+g_1(\eta)(1-\xi_j^2)+\cdots\right]$$
$$\cdot\left(\frac{1+\xi_j}{1-\xi_j}\right)^{1/2}\varphi_{CS}(\xi_j,\eta)\left[1+\frac{\bar{x}_i-\xi_j}{R_{ij}}\right]+\Psi_{GCS}(x_i,\chi,\eta) \tag{33b}$$

where

$$\Psi_{GCS}(x,\chi,\eta)=\sum_{p=0}^{1}\left[\phi_{CSp}(x,\chi)\psi_{Kp}(\bar{x},\bar{y},\eta)\right.$$
$$\left.-\sum_{a=1}^{ICS}\phi_{KCSp}(\xi_{Ca},\eta)\psi_{CSap}(\bar{y},\eta)\right] \tag{35}$$

$$\phi_{CS0}(x,\chi)=\left[g_0(\chi)+g_1(\chi)(1+x)+\cdots\right]\varphi_{CS}(x,\chi) \tag{36}$$

$$\phi_{CS1}(x,\chi)=\partial\phi_{CS0}(x,\chi)/\partial x \tag{37}$$

$$\psi_{CSa0}(\bar{y},\eta)=\{L_0(\xi_{Ca},\eta)-\frac{2\pi}{2J+1}\sum_{j=1}^{J}(1-\xi_j^2)^{1/2}$$
$$\cdot\ln|[(\xi_j-\xi_{Ca})^2+E_a^2]^{1/2}-E_a|\} \tag{38}$$

$$\psi_{CSa1}(\bar{y},\eta)=\{L_1(\xi_{Ca},\eta)-\frac{2\pi}{2J+1}\sum_{j=1}^{J}(1-\xi_j^2)^{1/2}(\xi_j-\xi_{Ca})$$
$$\cdot\ln|[(\xi_j-\xi_{Ca})^2+E_a^2]^{1/2}-E_a|\} \tag{39}$$

$$L_0(\xi_{Ca},\eta)=(1-\xi_{Ca})\ln|[(1-\xi_{Ca})^2+E_a^2]^{1/2}-E_a|$$
$$+(1+\xi_{Ca})\ln|[(1+\xi_{Ca})^2+E_a^2]^{1/2}-E_a|-E_a$$
$$\cdot\ln\left|\frac{\{[(1+\xi_{Ca})^2+E_a^2]^{1/2}+(1+\xi_{Ca})\}\{[(1-\xi_{Ca})^2+E_a^2]^{1/2}+(1-\xi_{Ca})\}}{E_a^2}\right|-2 \tag{40}$$

$$L_1(\xi_{Ca},\eta)=\xi_{Ca}+\frac{1}{2}\{(1-\xi_{Ca})^2\ln|[(1-\xi_{Ca})^2+E_a^2]^{1/2}-E_a|$$
$$-(1+\xi_{Ca})\ln|[(1+\xi_{Ca})^2+E_a^2]^{1/2}-E_a|\}$$
$$-\frac{1}{2}E_a\{[(1-\xi_{Ca})^2+E_a^2]^{1/2}-[(1+\xi_{Ca})^2+E_a^2]^{1/2}\} \tag{41}$$

$$\phi_{KCS0}(\xi_{Ca},\eta)=\left\{\left[g_0(\eta)+g_1(\eta)(1+\xi)+\cdots\right]\left[1+\frac{\bar{x}-\xi}{R}\right]\right\}_{\xi=\xi_{Ca}} \tag{42}$$

$$\phi_{KCS1}(\xi_{Ca},\eta)=\left[\frac{\partial}{\partial\xi}\phi_{KCS0}(\xi,\eta)\right]_{\xi=\xi_{Ca}} \tag{43}$$

The expression for downtream distribution of $\alpha = 0, \delta \neq 0$ is obtained by using Equations (31), (32), (33b) and (34b):

$$\begin{aligned}
\frac{W_{CSK}(\bar{x}_i, \bar{y}_r)}{4\rho U_\infty^2} = & -\frac{2\pi^2}{S(2J+1)} \sum_{i=1}^{s} \sum_{l=1}^{J} \frac{1-\eta_l^2}{(\bar{y}_r - \eta_l)^2} \\
& \cdot \{[g_0(\eta_l)(1-\xi_i) + g_1(\eta_l)(1-\xi_i^2) + \cdots] \\
& \cdot \left(\frac{1+\xi_i}{1-\xi_i}\right)^{1/2} \varphi_{CS}(\xi_i, \eta_l) + [g_{JC}(\eta_l)(1-\xi_i) + g_{(JC+1)}(\eta_l)(1-\xi_i^2) + \cdots]\} \\
& \cdot \left[1 + \frac{\bar{x}_i - \xi_i}{\sqrt{(\bar{x}_i - \xi_i)^2 + \beta^2(\bar{y}_r - \eta_l)^2}}\right] + \frac{2\pi^2 S}{2J+1} \sum_{l=1}^{J} \\
& \{[g_0(\bar{y}_r)(1-\xi_i) + g_1(\bar{y}_r)(1-\xi_i^2) + \cdots]\left(\frac{1+\xi_i}{1-\xi_i}\right)^{1/2} \\
& \cdot \varphi_{CS}(\xi_i, \bar{y}_r) + [g_{JC}(\bar{y}_r)(1-\xi_i) + g_{(JC+1)}(\bar{y}_r)(1-\xi_i^2) + \cdots]\} \\
& \cdot \left[1 + \frac{\bar{x}_i - \xi_i}{|\bar{x}_i - \xi_i|}\right] - \frac{\pi}{S} \sum_{i=1}^{s} \frac{(1-\eta_i^2)}{(\bar{y}_r - \eta_i)^2} [\Psi_{CCS}(\bar{x}_i, \bar{y}_r, \eta_i) + \Psi_{CK}(\bar{x}_i, \bar{y}_r, \eta_i)] \\
& + \pi S[\Psi_{CCS}(\bar{x}_i, \bar{y}_r, \bar{y}_r) + \Psi_{CK}(\bar{x}_i, \bar{y}_r, \bar{y}_r)]
\end{aligned} \tag{44}$$

The un-explained symbols in this section, with the exception of $\phi_{m0}(\bar{x}, \bar{y}) = \left(\frac{1-\bar{x}}{1+\bar{x}}\right)^{1/2} [g_{JC}(\bar{y}) + g_{(JC+1)}(\bar{y})(1+\bar{x}) + \cdots]$, are identical to those in the last section.

3. Determination of the undetermined coefficients a_{nm}

We write Equations (29) or (44) as a matrix equation:

$$[(A_{nm})_{ir}]\{a_{nm}\} = -\pi \left\{\frac{\partial Z_{ir}}{\partial \bar{x}}\right\} \tag{45}$$

where $\{a_{nm}\}$ and $\left\{\frac{\partial Z_{ir}}{\partial \bar{x}}\right\}$ are column matrices; $\frac{\partial Z_{ir}}{\partial \bar{x}}$ is the boundary condition at the optimal downstream point $(\underline{x}_i, \underline{y}_r)$, i.e., the inclination of the object surface; $[(A_{nm})_{ir}]$ is the matrix. The elements of the matrix may be obtained from Equations (29) or (44).

After a_{nm} are solved from Equation (45), the lift distributions and the other aerodynamic quantities of the wing surface and the

control surfaces under given conditions may then be found from Equations (4) or (7).

VI. SAMPLE CALCULATION AND CONCLUSIONS

The above computational method has been coded into a program for the X-2 computer. Calculation shows that the numerical results of our method agree well with experimental data with the same accuracy as other theoretical values. Figure 3 shows one sample calculation, which requires only two minutes of machine time on a 709 computer.

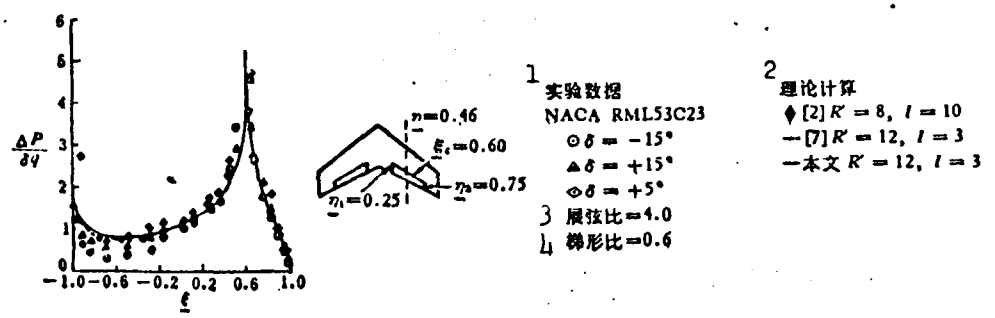

Figure 3. Comparison of the computed values in this paper to the experimental data and other theoretical values $(M_\infty=0.6,\ \eta=0.46)$

Key: 1--experimental data; 2--theoretical calculation; 3--ratio of lateral to tangential dimensions; 4--trapezoidal ratio

From the limited numerical results, it has been demonstrated that the method presented in this paper is reliable. Compared to the vortex lattice method, our method requires only a few downstream points, thus greatly reducing the machine stroage requirement and computational time. The numerical computation may be carried out on small computers.

REFERENCES

[1] Hedman, S. G., Vortex Lattice Method for Calculation of Quasi Steady State Loadings on Thin Elastic Wings in Subsonic Flow, FFA Report 105 (1966).
[2] Alkano, E. and Rodden, W. P., *AIAA Journal*, 7, 2 (1969)
[3] Landahl, M., *AIAA Journal*, 6, 2 (1968). 345—349.
[4] Ashley, H. and Rowe, W. S., *Z. Flugwissenschaften*, 18, 9—10 (1970).
[5] Zwaan, R. J., On a Kernel-Function Method for the Calculation of Pressure Distributions on Wings with Harmonically Oscillating Control Surfaces in Subsonic Flow, NLR TR 70123U (1971).
[6] Rowe, W. S., Winther, B. A. and Redman, M. C., *J. Aircraft*, 11, 1 (1974), 45—54.
[7] Cunningham, A. M., Jr., *J. Aircraft*, 9, 6 (1972), 413—419.
[8] Cunningham, A. M., Jr., *J. Aircraft*, 8 ,3 (1971), 168—176.
[9] Theodorsen, Th., General Theory of Aerodynamic Instability and the Mechanism of Flutter, NACA TR 496 (1934).
[10] Hsu, P. T., Some Recent Developments in the Flutter Analysis of Low-Aspect-Ratio Wings, National Specialists Meeting Proceedings, Dynamics and Aeroelasticity (1958), 7—26.
[11] Kopal, Z., Numerical Analysis, Second edition, London (1961), 382—384.

ON THE KERNEL FUNCTION COLLOCATION METHOD IN STEADY SUBSONIC FLOW FOR WING WITH CONTROL SURFACES

Chen Jing-song

(Nanjing Aeronautical Institute)

Abstract

In this paper, the forms of lift distribution function for wings with control surfaces in steady subsonic flow are analysed. The methods for treating the singularities which occur in the kernel of linear integral equation and in the lift distribution functions are also discussed, with the numerical solution of the integral equation given. The method proposed may be used to calculate the lift distribution of the wing alone and of the wing with full or partial span control surfaces on both the leading and the trailing edge. The numerical results are in good agreement with experimental data, and are as accurate as those obtained by other theories. As compared with the vortex-lattice method, both the required computing time and the computer capacity are reduced. Thus, the numerical calculations may be carried out on smaller computers.

ON THE CAPACITY OF HOLOGRAPHIC PHASE-SHIFT INTERFEROMETRIC TECHNIQUE IN THE VISUALIZATION OF LOW DENSITY FLOWS*

Li Hua yu, Xu Chao yi, Shu Jiau, Hu Jin min
(Institute of Mechanics, Academia Sinica)

ABSTRACT

Gas flows at high Mach numbers are usually associate with very low gas density, especially in simulating flight conditions at high altitudes. In visualizing such flows the question usually arises as to how the sensitivity of the optical method may be increased.

Paper [2] has pointed out that, if the reference beam of holography has a certain phase-shift between the two exposures, a higher sensitivity can be achieved. Paper [2] appends an experimental result in which the phase-shift value is $\pi/2$. The present paper analyses the phase-shift interferometric technique in detail. According to this analysis, when the phase-shift value is $\pi/2$, a resolution limit about $\lambda/1000$ can be achieved. This is 25.4 times higher than the common double-exposure holographic method in which the phase-shift value is zero. Furthermore, the present paper points out that when the phase-shift value increases from $\pi/2$ to π, the sensitivity also increase monotonously (for instance, when the phase-shift value is $0.89\,\pi$, a resolution limit about $\lambda/6000$ can be achieved). The optimum phase-shift value is probably near π.

This paper presents some experimental results of a low density flow. Some problems in application of this technique are discussed.

*Received February 19, 1978

A highly sensitive holographic interferometric method deserving our attention is introduced in this paper. As pointed out in [2], the sensitivity may be raised when there is a phase shift in the reference beam between the two exposures in holographic interferometry. The experimental results for a phase shift of $\pi/2$ is also reported in that paper. In this paper, we analyze in detail the interferometric technique and point out that at a phase shift of $\pi/2$, this method may achieve a resolution of about 1/1000 wave length, 25.4 times the sensitivity of ordinary double exposure holographic technique (with 0 phase shift). It is also noted that the sensitivity may be further improved for phase shift greater than $\pi/2$ and smaller than π, the best phase shift value being in the neighborhood of π. We append in this paper the experimental result for a low density flow to demonstrate the ability of this method in visualizing low density variable flow field and discuss some of the problems encountered in its application.

The finite fringe interferometric method used in the investigation of flow fields has generally a resolution of about 1/20 wave length. In practice, there exists a great number of situations where the state of matter has a variation much less than 1/20 wave length, such as the study of supersonic air flow, all kinds of low speed flows, small cross-section tube flow, etc. Hence the improvement of the sensitivity of the interferometric technique has always been an important research topic. The phase complementation method of [1] is an outstanding example of works in this area. In that paper, a highly sensitive visualization method has been developed by applying the principle of spatial complex filtered wave, including the application of the phase shift technique.

In contrast to the principle of spatially filtered waves with phase shift only in local waves, [2] introduced the technique of phase shift for the whole wave to improve sensitivity by changing the phase of the reference beam between the two exposures of the hologram. It also exhibited the pictures taken with the high

sensitivity obtained after shifting the phase by $\pi/2$. [3] applied similar principles in non-holographic situations to realize a high sensitivity in ordinary interferometric methods by controlling the initial phase difference between the two interfering beams to be around $\pi/2$.

We discussed the phase shift technique in the holographic interferometric method in an attempt to explain the physical interaction of the phase shift method and the relationship between the phase shift value and the sensitivity of the measurement. We also compare the methods in [2,3] and note that the best possible phase shift value is not $\pi/2$, but is close to π. The experimental results are included in the appendix with a discussion of the problems that exist in the application.

I. ANALYSIS OF THE PHASE SHIFT TECHNIQUE

1. Effect of changing the phase of the reference beam between the two exposures during flow field visualization on the double exposure hologram

Let the object wave at the first exposure be $e^{iO(x,y)}$, the reference wave be $e^{iR(x,y)}$, the object wave at the second exposure be changed to $e^{i[O(x,y)+\varphi(x,y)]}$, the reference wave be $e^{i[R(x,y)+c]}$, where φ is the phase change caused by the flow field and c is the phase shift value.

Assume that the recording medium records the intensity linearly [1], then according to the general theoretical treatment, the following conclusion may be arrived at: (1) even if the medium should be non-linear, the following discussion will not be affected because in the off-axis holography, the non-linear effect only produces higher order diffraction images with large diffraction angles. It is separate spatially from the first order image that is to be used. When the processed hologram is illuminated with reference

R(x,y), the two objective waves emitted are respectively $e^{i\varphi(x,y)}$ and $e^{i[\varphi(x,y)+\varphi(x,y)-c]}$. c = 0 is the situation for ordinary double exposures. This conclusion indicates that during the second exposure, the increased phase c of the reference beam is equivalent to: (1) the phase c subtracted from the measured objective wave in the ordinary double exposure holographic interferometry; (2) the uniform initial phase difference c in the whole interfering plane of the two interfering waves in non-holographic interference.

2. Intensity distribution of low density flow interferogram (flow field that only induces small phase changes)

The intensity distribution of two beam interferogram is

$$I(x,y) = \frac{I_0}{2}\{1 + \cos[\varphi(x,y) - c]\} \tag{1}$$

where I_o is the intensity at $\varphi = 0$ when c = 0, i.e., the background intensity of the interferogram when c = 0. The words (x,y) will be omitted in the rest of this paper.

Omitting all terms above φ^2 under the condition of weak phase changes, we get

$$I(x,y) = \frac{I_0}{2}\left[(1 + \cos c) + \varphi \sin c - \frac{\varphi^2}{2}\cos c\right] \tag{2}$$

From the above equation, the distribution of I(x,y) when $c = 0, \pi/2,$ is as follows:

$$\left.\begin{aligned} I(x,y) &= I_0\left(1 - \frac{\varphi^2}{4}\right) \quad \text{for } c = 0 \\ I(x,y) &= \frac{I_0}{2}(1 + \varphi) \quad \text{for } c = \pi/2 \\ I(x,y) &= \frac{I_0}{4}\varphi^2 \quad \text{for } c = \pi \end{aligned}\right\} \tag{3}$$

The background intensity of the interferogram may be expressed as

$$I(x,y)|_{\varphi=0} = \frac{I_0}{2}(1 + \cos c) \tag{4}$$

This is a parameter used to discuss sensitivity and a function of c

$$\left.\begin{aligned} I(x, y)|_{\varphi=0} &= I_0 \quad \text{for } c = 0 \\ I(x, y)|_{\varphi=0} &= \frac{I_0}{2} \quad \text{for } c = \pi/2 \\ I(x, y)|_{\varphi=0} &= 0 \quad \text{for } c = \pi \end{aligned}\right\} \tag{5}$$

Besides, we define the intensity enhancement ΔI by the following definition:

$$\Delta I = I(x, y) - I(x, y)|_{\varphi=0} = \frac{I_0}{2}\left(\varphi \sin c - \frac{\varphi^2}{2}\cos c\right) \tag{6}$$

3. Relationship between the phase shift c and the observed sensitivity

The flow field interferogram contrast is defined by

$$M = \frac{\Delta I}{I|_{\varphi=0}} = \frac{\varphi \sin c - \frac{\varphi^2}{2}\cos c}{1 + \cos c} \tag{7}$$

This function is monotonic when $c < \pi$. When $c = \pi$, $M = \infty$. But due to the effects of scattering and diffraction, etc., there exists randomly light so that $I|_{\varphi=0}$ will never be zero to produce an absolutely dark background. Thus practically $M \neq \infty$). From the contrast angle, naturally the sensitivity is higher when $c = \pi$. But, the intensity enhancement should also be a practical factor to be considered because when φ is very small, ΔI will also be very small, making it possibly too small to be recorded. In the following we will further investigate the relationship between ΔI and c.

From Equation (6), we know that ΔI has a very large value when $c = \mathrm{tg}^{-1}(-2/\varphi)$ (when φ is very small, this condition is equivalent to $c \approx \pi/2$), and a very small value when c = 0 and in the vicinity of π. The difference may be seen from the following equation:

$$\left.\begin{aligned} \Delta I &= -\frac{I_0}{4}\varphi^2 \quad \text{for } c = 0 \\ \Delta I &= \frac{I_0}{4}\varphi^2 \quad \text{for } c = \pi \\ \Delta I &= \frac{I_0}{2}\varphi \quad \text{for } c = \pi/2 \end{aligned}\right\} \tag{8}$$

Summarizing the above discussions, we know that if there is no problem of recording ΔI, the best value of the phase shift is π. But if φ is very small, the recording of ΔI will be limited by the facts as pointed out by Equation (8), then the best phase shift practically should be determined by a compromise between the maximum value of M and the limiting value of ΔI; and this may fall between $\pi/2$ and π, depending on the actual experimental conditions. With the improvement of technology, the best phase shift value will approach π. For example, as pointed out in [4], the sensitivity may be improved by another 1-2 orders of magnitude if the light intensity is received directly with photoelectric.

4. Estimation of achievable sensitivity when $c = \pi/2$

1) Observable sensitivity: the smallest intensity variation that can be discerned in an interferogram by directly observing it with the human eye is called the observable sensitivity. It is generally accepted that $M = 1/100$ is the limit discernible by the human eye. From this may be obtained the smallest discernible phase shift. From Equation (7), we know

$$M|_{c=0} = -\varphi^2/4, \quad M|_{c=\pi/2} = \varphi \tag{9}$$

Substituting $M = \pm 1/100$ into the above, we get

$$\varphi_{min}|_{c=0} = \frac{2\pi}{31.4} \text{ for } \Delta L_{min}|_{c=0} = \frac{\lambda}{31.4}$$

$$\varphi_{min}|_{c=\pi/2} = \frac{2\pi}{626} \text{ for } \Delta L_{min}|_{c=\pi/2} = \frac{\lambda}{628}$$

where φ_{min} is the smallest discernible phase change, ΔL_{min} is the corresponding optical path differences, λ is the wave length. From this it can be seen that the sensitivity of the $c = \pi/2$ method is 20 times that of ordinary double exposure method.

2) Recordable sensitivity. The smallest density variation that can be discerned on the film when the interferogram is recorded photographically is called the recordable sensitivity. In practice

the sensitivity may be further improved by using high contrast film. But the processing requirement is more demanding: The exposure must be correct, the control on the γ value during developing must be strict to guarantee the linearity of the record and the necessary value of γ. Starting with the characteristic curve of the recording film (Figure 1), we have

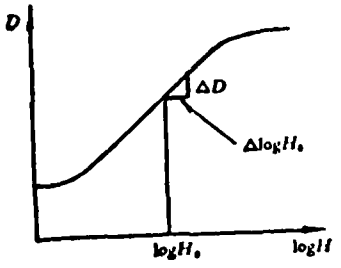

Figure 1. Characteristic curve of recording film

$$\Delta D = \gamma[\log(H_0 + \Delta H) - \log H_0] = 0.434\gamma \ln\left(1 + \frac{\Delta H}{H_0}\right) \approx 0.434\gamma \frac{\Delta H}{H_0} \quad (10)$$

$$\Delta H/H_0 = M \quad (11)$$

where D is the film density, H is the film exposure value, H_o is the film background exposure value, γ is the reverse difference coefficient of the film after developing, ΔH is the exposure value enhancement corresponding to ΔI, and ΔD is the density enhancement corresponding to ΔH. In Equation (10), the condition for the approximation is that $\Delta H/H_o$ is very small. Solving Equations (9)-(11) simultaneously, we get

$$\Delta D|_{c=0} = -0.434\gamma\frac{\varphi^2}{4}, \quad \Delta D|_{c=\pi/2} = 0.434\gamma q \quad (12)$$

Under the condition that $\Delta D|_{\text{discernible}} = 1/100$ [1], and γ = 4, we get

$$\varphi_{min}|_{c=0} = \frac{2\pi}{41.3}, \quad \Delta L_{min}|_{c=0} = \frac{\lambda}{41.3}$$

$$\varphi_{min}|_{c=\pi/2} = \frac{2\pi}{1090}, \quad \Delta L_{min}|_{c=\pi/2} = \frac{\lambda}{1090}$$

Thus, the sensitivity of the c = π/2 method is 26.4 times that of the ordinary double exposure method. In this discussion, the reason why the recordable sensitivity is higher than the observable sensitivity is that films with high γ value have been used (contrast Equations (9) and (12)). If $\gamma < 1/0.434 = 2.31$, then the recordable sensitivity will be lower than the observable sensitivity.

---

[1] D=log O, $O=F_o/F$ is called the optical resistivity. F_o is the incident light transmittance on the film when measuring D. F is the optical transmittance through the film. $\Delta D=\log(O/O_o)$. When ΔD= 1/1000, $O/O_o=1.023$.

$\gamma \approx 1$, for ordinary films, therefore, ordinarily the recordable sensitivity is considered to be lower.

The above method was also used in [3] to estimate the recordable sensitivity of its optical system. According to its estimate, the highest discernible value for its system is $\lambda/500$, exactly half of the value in our paper. The reason is that complementary double exposure was used in the system to compensate for the original error in the optical elements so that the background intensity could be made uniform. Thus, because the phase shift was fixed near $\pi/2$, ΔH was similar to that in our paper but H_o was doubled. Hence the highest discernible value is lowered by one half. Furthermore, holographic interferometric technique can maintain the same phase shift for every point in the flow field. The method in [3] could not achieve this due to error in the processing. Therefore, the sensitivity at each point of the flow field is different. The holographic method is also superior in this regard.

In theory, the sensitivity at phase shift $\pi/2$ is lower than that at phase shift π. But there are two advantages for phase shift $\pi/2$: 1) ΔI is largest, making it easier to record; 2) ΔI and φ are linearly related so that quantitative analysis is easier. Since its sensitivity is already high, this will improve its practical value.

5. Estimation of the sensitivity when c approaches π

Since we have only considered the effects of the major factors in our theory, we have reached the conclusion that $M = \infty$ when $c = \pi$. In reality, the closer is c to π, the greater are the effects of those factors not included in the theory. For example, when $M = \infty$, infinitesimally small ΔI can also be recorded. Here the exposure time should be infinitely long, but the fogginess of the film, the stray light during reconstruction and other factors

will make the recording meaningless. That is to say, if the φ that needs to be recorded is very small, then the best phase shift value must be smaller than π and must be a compromise between the limiting value of ΔI and the largest value of M. Two examples will be used below to estimate the recordable sensitivity.

1) The recordable sensitivity when c = 150°. By substituting $\gamma = 4$, $\Delta D = 1/100$ into Equations (7), (10) and (11), we get

$$\varphi_{min}|_{c=150^\circ} = \frac{2\pi}{5036}, \quad \Delta L_{min}|_{c=150^\circ} = \frac{\lambda}{5036}$$

The intensity enhancement is very small for such a small phase shift. We compare them as follows:

$$\Delta I|_{c=0,\pi,\varphi=2\pi/5036} = 7.784 \times 10^{-7} \times \frac{I_0}{2}$$

$$\Delta I|_{c=\pi/2,\varphi=2\pi/5036} = 1.248 \times 10^{-3} \times \frac{I_0}{2}$$

$$\Delta I|_{c=150^\circ,\varphi=2\pi/5036} = 6.254 \times 10^{-4} \times \frac{I_0}{2}$$

2) Recordable sensitivity when c = 160°. Similarly, the following data are obtained

$$\varphi_{min}|_{c=160^\circ} = \frac{2\pi}{6195}, \quad \Delta L_{min}|_{c=160^\circ} = \frac{\lambda}{6195}$$

$$\Delta I|_{c=0,\pi,\varphi=2\pi/6195} = 5.14 \times 10^{-7} \times \frac{I_0}{2}$$

$$\Delta I|_{c=\pi/2,\varphi=2\pi/6195} = 1.014 \times 10^{-3} \times \frac{I_0}{2}$$

$$\Delta I|_{c=160^\circ,\varphi=2\pi/6195} = 3.473 \times 10^{-4} \times \frac{I_0}{2}$$

It can, therefore, be seen that the sensitivity continues to improve and ΔI to decrease when the phase shift approaches π but when the phase shift deviates slightly from π, the value of ΔI

will be increased greatly over its value at $c = \pi$, thus reaching a stage where it may be usable.

II. RESULTS AND EXPERIMENTAL SET-UP

1. Experiment set-up

The following experiment was performed to investigate the feasibility of applying the phase shift interferometric technique in the visualization of low density flow field. The object of the experiment is a small column of freely flowing air, passing through a tube under constant total pressure of 700 mm Hg in a container into a cylindrical exhaust tube of diameter 1 mm and length 4 mm and then into the atmosphere. The commonest off-axis holygraphic optical path is used (Figure 2). The phase shift is achieved by using a phase regulator in the path of the reference beam prior to beam-expansion

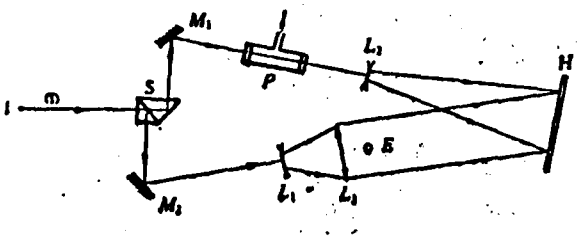

Figure 2. Diagram of experimental optical path.
(1) HeNe laser beam; H holographic plate; S beam divider; M_1M_2 total reflecting mirrors; L_1L_2 beam expanding lenses; L_3 parallel focusing lens; P phase regulator; E exhaust tube

The phase regulator is a ϕ12mm × 100mm metal cavity with the two ends sealed by optical glass. The pressure in the cavity is very stably controlled by a two stage pressure stabilizer.

The various phase shift values c = 0, $\pm\pi/2$, π are achieved conveniently by controlling the pressure value. The sign of the phase shift is determined by filling the phase regulator with air either during the first or the second exposure. The distortion of the optical glasses at the two ends of the phase regulator should be minimized in the design of the regulator. This problem is solved in our case by controlling the length of the metal cavity. Two factors are taken into consideration: 1) the applied pressure should be minimized. A pressure of only 60 mm H_2O is required to achieve a phase shift of $\pi/2$ in our regulator (at room temperature 20°C) [1]; 2) the air pressure should be within the operating range of the pressure stabilizer. Therefore, the cavity cannot be too long. There are other schemes for the phase regulator. For example, the piezoelectric crystal is also a possibility.

2. Experimental results

Experiment indicates that the observed sensitivity can really be greatly improved with the phase shift technique. Limited by circumstances, we recorded with ordinary aeronautic microfilm with no control on the γ value. The recordable sensitivity is lower than the observable sensitivity and far lower than the standard in the above discussion. For results, please refer to the pictures 1-6 in Plate I. Picture 1: Recorded with the ordinary double exposure method. A very short dark flow column could be vaguely discerned during observation. Nothing can be seen in the photographic record. Picture 2: Recorded by the finite fringe double exposure method. The limited fringes are produced by the liquid wedge. A disturbance with an optical path difference of about $\lambda/10$ can be seen at the exit of the flow column. The bending at

---

[1] The pressure required for phase shift $\pi/2$ may be calculated with the following formula:

$$p = \frac{1}{4}\frac{\lambda p_0}{KL}\frac{T}{T_0}$$

where $K=2.94 \times 10^{-4}$, L is the length of the cavity, T is absolute temperature, p_0, T_0 are the pressure and absolute temperature at STP. After substituting in the values, we have $p_{relative} = 0.0204T$, dimension being mm H_2O.

the second fringe is already very small. Pictures 3 and 4: Recorded by the double exposure method with phase shift $\pm\pi/2$. A white (corresponding to a phase shift $\pi/2$) and a dark (corresponding to a phase shift of $\pi/2$) flow column can be individually observed clearly within a fairly long range. The visualization capability is much higher than that in pictures 1 and 2. Picture 5: Recorded by the double exposure method with phase shift π. A white flow column over a dark blackground can be seen. Picture 6: The experiment was disturbed by some unusual factors, but they accidentally make the phase shift in the flow region come out to be ideally π. The resulting visualization of the flow is the best.

We also tested the operation of the phase regulator in real time. When the pressure is increased continuously, the fringes continue to scan with the value of position shift in agreement with calculated value. Therefore, it has operated normally.

3. Discussion of existing problems

In practical applications, a serious impediment of our method is the stringent requirement on the environment. The experiment in our paper had been performed over 80 times with satisfactory results in only a few cases. The reason is that the disturbance of the surrounding can easily exceed $\pi/2$ (e.g., air flow, thermal disturbance, small vibrations,...) so that the desired phase shift value cannot be achieved, leading to the failure of the experiment or to disturbances of various degree. If we use the single exposure hologram as a wave memory storage and then use it for image reconstruction with the phase shift method in a better environment may be a successful way to do this experiment. This technique has a good prospect. Its development awaits future practices.

The second problem is that there still exists certain difficulties in using this technique in quantitative measurement. But if the error can be reduced, then by using the linear relationship between intensity and phase, the quantitative measurement may be achieved with a micro-densitometer.

IV. CONCLUSIONS

The special feature of the method in this paper is its high sensitivity and theoretical simplicity. Concerning the latter, we have not seen any paper discussing it, probably because that it is difficult to achieve in practice. Theoretically, the difficulty to achieve constant phase shift has been eliminated with the appearance of holographic photography. Hence, it can be predicted that the high sensitivity of our method will find its use in a suitable field.

REFERENCES

[1] Zernike, F., *Z. Tech. Phys.*, 16 (1935), 454.

[2] Velzel, C. H. F., Small phase differences in holographic interferometer, Application De L'Holographic, Proc. of the Inter. Symp. of Holo. (1970).

[3] Smeets, G., et al., Interferograms of high optical quality by double exposure, Proc. of the 10th Inter. Congr. on High-Speed Photography (1972), 244.

[4] Schall, R., New laser high-speed measurement techniques in aerodynamics, Proc. of the 11th Inter. Congr. on High-Speed Photography (1974), 41.

ANALYTICAL DESIGN FOR INTERNAL BURNING STAR GRAINS OF SOLID ROCKETS*

Lü Changtang

For the design of the internal burning star grains of solid rocket motors, in the past people usually carried out pure geometric research and the corresponding trial and error method. The formulae and computational curves in [1] are typical. They are widely used in the engineering design and scientific education in foreign countries. Practical experience shows that the pure geometric formulae and curves in [1] are complex and numerous and yet incomplete; the corresponding trial and error method not only involves large volumes of computation, but is also uncertain, difficult to guarantee the accuracy of various specifications and to achieve, in particular, the optimal design standard. In this paper, we try to use analytic design instead of trial and error. Different from the traditional pure geometric research, we organically combine the various geometric parameters of the internal burning star grain, the various characteristic parameters of solid propellant, and the technical specifications of the rocket motor together, establish the set of design equations according to the best principle of grain design, and then solve the set of equations quickly by incorporating simple equations and curves. Compared with [1-3], our method not only involves less computational work and guarantees the required technical specifications but also yields a design that approaches the optimal, improves the characteristics of the rocket motor, saves

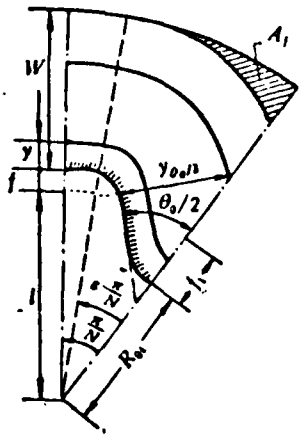

Figure 1. Diagram of design unit for the internal burning star grain

*Received April 25, 1978

materials and requires less difficult work on the computer.

1. The geometric functional relations of the internal burning star grain

As in Figure 1, it is not difficult to obtain the functional relationship between the geometric parameters of the internal burning star grain according to Piobert's combustion law as done in [1]. For simplicity in the calculation, we first give below only the function k (Figure 2) and function s_o (for the meaning of symbols, see Figure 1) which are only related to N, the number of points in the star and $\theta_o/2$, the initial half angle of the star

$$k = 2N\left(\frac{\pi}{2} + \frac{\pi}{N} - \frac{\theta_0}{2} - \operatorname{ctg}\frac{\theta_0}{2}\right) \tag{1}$$

$$s_0 = 2Nl\,\frac{\sin\varepsilon\frac{\pi}{N}}{\sin\frac{\theta_0}{2}} + 2\pi l(1-\varepsilon) + kf \tag{2}$$

From these, the combustion surface A_{b1} in the first stage and the initial port area A_{pol} may be simplified into the two equations below:

$$A_{b1} = L_p[s_0 + kf_1 + 2\pi(y - f_1)] \tag{3}$$

$$A_{po1} = s_0 f + l^2 c + \pi f_1^2 - 0.5k(f^2 + f_1^2) \tag{4}$$

where L_p is the grain length. For other symbols, see Figure 1. For value of c, see the equation below:

$$c = (1-\varepsilon)\pi + N\sin\varepsilon\frac{\pi}{N}\cos\varepsilon\frac{\pi}{N} - N\sin^2\varepsilon\frac{\pi}{N}\operatorname{ctg}\frac{\theta_0}{2} \tag{5}$$

From analysis, we know that angle $\theta/2$, called the dynamic angular variable, increases monotonically in the interval $[\theta_0/2, \theta_w/2]$ with the combustion time, starting from $y\theta_o/2$, the star edge vanishing point. $\theta_w/2$ is the star half angle at the end of combustion. $\theta/2$ is related to the time-varying y as follows:

$$\frac{\theta}{2} = \arccos\frac{\sin\varepsilon\frac{\pi}{N}}{(y+f)/l} \tag{6}$$

By using the dynamic angular variable $\theta/2$, the second stage combustion area A_{bll} and the remaining grain area A_l may be simplified into the following functional forms:

$$A_{bll} = L_p\left[2\pi + 2N\left(\frac{\pi}{2} - \frac{\theta}{2}\right)\right]\frac{l \cdot \sin\varepsilon\frac{\pi}{N}}{\cos(\theta/2)} + 2\pi l L_p(1-\varepsilon) \tag{7}$$

$$A_l = \pi l(D_p - l)\varepsilon + N(W+l)^2\left(\frac{\theta_w}{2} - \frac{\pi}{2} - \sin\frac{\theta_w}{2}\cos\frac{\theta_w}{2}\right) - Nl^2\sin\varepsilon\frac{\pi}{N}\cos\varepsilon\frac{\pi}{N} \tag{8}$$

where the remaining grain surface star half angle $\theta_w/2$ at the end of combustion is

$$\frac{\theta_w}{2} = \arccos\frac{\sin\varepsilon\frac{\pi}{N}}{(W+l)/l} \tag{9}$$

It can be shown from mathematical analysis that A_{bll} has a minimum value A_{bmin} at $\bar{\theta}/2$ and is infinite stiffness form (Figure 3 is the functional curve of its infinite stiffness form) is

$$\frac{A_{bmin}}{l} = 2N\frac{\sin\varepsilon\frac{\pi}{N}}{\sin(\theta/2)} + 2\pi(1-\varepsilon) \tag{10}$$

Similarly, it may be proved that A_l has a minimum value A_{fmin} at $\frac{\theta_w}{2} = \frac{\pi}{2} - \varepsilon\frac{\pi}{N}$ i.e., $\frac{W+l}{l} = 1$

$$A_{fmin} = 2l^2\left(\pi\varepsilon - 2N\sin\varepsilon\frac{\pi}{N}\cos\varepsilon\frac{\pi}{N}\right) \tag{11}$$

The existence of A_{bmin} and A_{fmin} is an important feature of internal burning star grain.

The effective grain area A_{c0} when there is no star circular angle, namely $f_1 = 0$, is very important to the establishment and solution of the design equations. The following formula gives its value:

$$A_{c0} = \frac{\pi}{4}D_p^2 - \pi l(2f+l) - 0.5f^2k - 2\pi Wl\varepsilon - \frac{2Nfl}{\sin(\theta_0/2)}\sin\varepsilon\frac{\pi}{N} + Nl^2\operatorname{ctg}\frac{\theta_0}{2}\sin^2\varepsilon\frac{\pi}{N} - N(W+f)^2\cdot\left(\frac{\theta_w}{2} - \frac{\pi}{2} - \sin\frac{\theta_w}{2}\cos\frac{\theta_w}{2}\right) \tag{12}$$

Then the effective grain area A_{c01} when there is star circular angle, namely $f_1 \neq 0$ is

$$A_{c01} = A_{c0} - 0.5(2\pi - k)R_1^2 \tag{13}$$

The minimum radius R_o of the internal burning star grain when $f_1 = 0$ gives the governing relationship between the geometric parameters of the star grain. Since it is always true that $\frac{d(R_o/l)}{d\varepsilon} < 0$, therefore, R_o is a decreasing function of the angular coefficient ε. Let $R_o > 0$, then the upper limit ε_{Nap} of ε is:

$$\varepsilon_{N\Sigma} = \frac{N}{\pi}\left(\arcsin\frac{l}{l} + \frac{\theta_0}{2}\right) \tag{14}$$

Whenever $\varepsilon < \varepsilon_{N\Sigma}$, then $R_o > 0$ and $R_{o1} > 0$ (when $f_1 \neq 0$).

2. Establishment of the set of grain design equations

The known conditions are:

1) The required technical specifications for the motor: The total impuse I_t or required range, law of propulsion F_{min}-F_{max} operating time t_{min}-t_{max}, operating temperature T_{min}-T_{max}°C and the outer diameter D of the rocket motor or its limit, etc.

2) Property of solid propellant: specific impulse I_{sp}, combustion rate $\gamma = ap^n$, temperature coefficient α_T, limit of air current sensitivity coefficient k_{kp}, propulsion coefficient C_F, characteristic speed c^*, critical pressure P_{kp}, specific gravity ρ, etc.

The optimal grain design principle obeyed by the set of design equations: to be able to guarantee the relization of the total impulse, propulsion power requirement, operating work, etc; to be able to burn steadily and normally; to have a large effective grain coefficient η_c and a small coefficient η_f, etc. The stresses

under conditions permitted by the grain stress.

Thus, the design equation that guarantees the requirement total impulse of the rocket motor is

$$L_p[A_{p0} - 0.5(2\pi - k)f_1^2] = V_c \tag{17}$$

The design equation guaranteeing the value of the lower limit of propulsion power is

$$2N\left[\frac{\sin\varepsilon\frac{\pi}{N}}{\sin\frac{\theta}{2}} + (1-\varepsilon)\frac{\pi}{N}\right] = \frac{A_{bmin}}{lL_p} \tag{18}$$

The design equation guaranteeing the initial peak pressure limit for safe, stable combustion is

$$\frac{[s_0 - (2\pi - k)f_1]L_p}{A_{p0} + 0.5(2\pi - k)f_1^2} = \kappa_{xp} \tag{19}$$

By eliminating the grain length L_p and f_1 and substituting into the above Equations (1), (2), (8) and (12), the equation of the angular coefficient ε may be obtained

$$\begin{aligned}
&\frac{\pi}{4}\kappa_{xp}D_p^2 - \pi\kappa_{xp}l\varepsilon(D_p - l) - N\kappa_{xp}(W+f)^2\left[\arccos\frac{l\sin\varepsilon\frac{\pi}{N}}{W+f} - \frac{\pi}{2}\right.\\
&\left. - \frac{l\sin\varepsilon\frac{\pi}{N}}{W+f}\sin\left(\arccos\frac{l\sin\varepsilon\frac{\pi}{N}}{W+f}\right)\right] + N\kappa_{xp}l^2\sin\varepsilon\frac{\pi}{N}\cos\varepsilon\frac{\pi}{N} - \kappa_{xp}V_cA_{bmin}^{-1}2\pi l(1-\varepsilon)\\
&- 2NA_{bmin}^{-1}lV_c\kappa_{xp}\frac{\sin\varepsilon\frac{\pi}{N}}{\sin\frac{\theta}{2}} - \left[2Nl\frac{\sin\varepsilon\frac{\pi}{N}}{\sin\frac{\theta}{2}} + 2\pi l(1-\varepsilon)\right]^{-1}\cdot\left[2NlA_{bmin}\frac{\sin\varepsilon\frac{\pi}{N}}{\sin\frac{\theta_0}{2}}\right.\\
&\left. + 2\pi lA_{bmin}(1-\varepsilon) + 2NfA_{bmin}\left(\frac{\pi}{2} + \frac{\pi}{N} - \frac{\theta_0}{2} - \operatorname{ctg}\frac{\theta_0}{2}\right)\right]\\
&+ A_{bmin}\left[2Nl\frac{\sin\varepsilon\frac{\pi}{N}}{\sin\frac{\theta}{2}} + 2\pi l(1-\varepsilon)\right]^{-1}\cdot\left\{\pi^2D_p^2 - 4\pi^2l(2f+l)\right.\\
&\left. - 2\pi f^2\left(N\pi + 2\pi - 2N\frac{\theta_0}{2} - 2N\operatorname{ctg}\frac{\theta_0}{2}\right) - 8\pi^2lW\varepsilon - \frac{8\pi Nfl}{\sin\frac{\theta_0}{2}}\sin\varepsilon\frac{\pi}{N} + 4\pi Nl^2\operatorname{ctg}\frac{\theta_0}{2}\right.
\end{aligned} \tag{20}$$

$$\times \sin^2\varepsilon\frac{\pi}{N} - 4\pi N(W+f)^2\left[\arccos\frac{l\sin\varepsilon\frac{\pi}{N}}{W+f} - \frac{\pi}{2} - \sin\left(\arccos\frac{l\sin\varepsilon\frac{\pi}{N}}{W+f}\right)\frac{l\sin\varepsilon\frac{\pi}{N}}{W+f}\right]$$

$$- 4\pi V_c A_{b\min}\left[2Nl\frac{\sin\varepsilon\frac{\pi}{N}}{\sin\frac{\theta}{2}} + 2\pi l(1-\varepsilon)\right]^{-1} - \frac{\pi}{2}ND_p^2\cdot\left(\frac{\pi}{2}+\frac{\pi}{N}-\frac{\theta_0}{2}-\operatorname{ctg}\frac{\theta_0}{2}\right)$$

$$+ 2\pi Nl(2f+l)\cdot\left(\frac{\pi}{2}+\frac{\pi}{N}-\frac{\theta_0}{2}-\operatorname{ctg}\frac{\theta_0}{2}\right) + 2N^2f^2\left(\frac{\pi}{2}+\frac{\pi}{N}-\frac{\theta_0}{2}-\operatorname{ctg}\frac{\theta_0}{2}\right)^2$$

$$+ 4\pi NlW\varepsilon\left(\frac{\pi}{2}+\frac{\pi}{N}-\frac{\theta}{2}-\operatorname{ctg}\frac{\theta}{2}\right) + 4N^2fl\left(\frac{\pi}{2}+\frac{\pi}{N}-\frac{\theta_0}{2}-\operatorname{ctg}\frac{\theta_0}{2}\right)$$

$$\times\frac{\sin\varepsilon\frac{\pi}{N}}{\sin\frac{\theta_0}{2}} - 2N^2l^2\left(\frac{\pi}{2}+\frac{\pi}{N}-\frac{\theta_0}{2}-\operatorname{ctg}\frac{\theta_0}{2}\right)\operatorname{ctg}\frac{\theta_0}{2}\cdot\sin^2\varepsilon\frac{\pi}{N} + 2N^2(W+f)^2 \qquad (20)$$

$$\times\left[\arccos\frac{l\sin\varepsilon\frac{\pi}{N}}{W+f} - \frac{\pi}{2} - \sin\left(\arccos\frac{l\sin\varepsilon\frac{\pi}{N}}{W+f}\right)\frac{l\sin\varepsilon\frac{\pi}{N}}{W+f}\right]\left(\frac{\pi}{2}+\frac{\pi}{N}-\frac{\theta_0}{2}-\operatorname{ctg}\frac{\theta_0}{2}\right)$$

$$+ 2NV_cA_{b\min}^{-1}\cdot\left(\frac{\pi}{2}+\frac{\pi}{N}-\frac{\theta_0}{2}-\operatorname{ctg}\frac{\theta_0}{2}\right)\left[2\pi l(1-\varepsilon)+2Nl\frac{\sin\varepsilon\frac{\pi}{N}}{\sin\frac{\theta}{2}}\right]\Bigg\}^{-1} = 0\ (20)$$

It may be seen that this equation contains simultaneously all the factors such as the required technical specifications, the property of the propellant and genetric parameters of the internal burning grain, etc.

3. Requirement of the design equations and obtaining the geometric parameter of the grain

Obviously, it is difficult to solve for ε in Equation (20). We change it into two functional curves Y_1, Y_2 with ε as the variable:

$$Y_1 = \kappa_{sp}\left(\frac{\pi}{4}D_p^2 - A_l - \frac{V_c}{L_p}\right),\quad Y_2 = L_p[t_b - \sqrt{2\Delta(2\pi - k)}] \qquad (21)$$

where

$$\Delta \equiv A_\infty - (V_c/L_p) \qquad (22)$$

The necessary equation with Δ as solution can only be solved when $\Delta \geqslant 0$.

For each positive integer N, the angle $\theta_0/2$ has an upper limit $\theta_{Nk}/2$ that makes Δ = 0 and $f_1 = 0.\theta_{Nk}/2$, is an increasing function

of N, therefore, the angle $\theta_o/2$ must be within the interval $(0, \theta_{N\mu p}/2)$ and be determined according to the initial power requirement. N and $\theta_o/2$ are called the parametric variables of Equation (20). To obtain good overall grain property, the values of N and $\theta_o/2$ should be used (such as $N = 2,3, \theta_o/2 = 10°$). After N and $\theta_o/2$ are fixed, use $(N, \theta_o/2)$ to search k value from Figure 2 and then calculate the curves Y_1, Y_2 of ε: For each ε selected, find the value of s_{min}/l from Figure 3 with (N, ε) and substitute into the following equation to get L_p:

$$L_p = \frac{A_{\Delta min}}{l \cdot \frac{s_{min}}{l}} \tag{23}$$

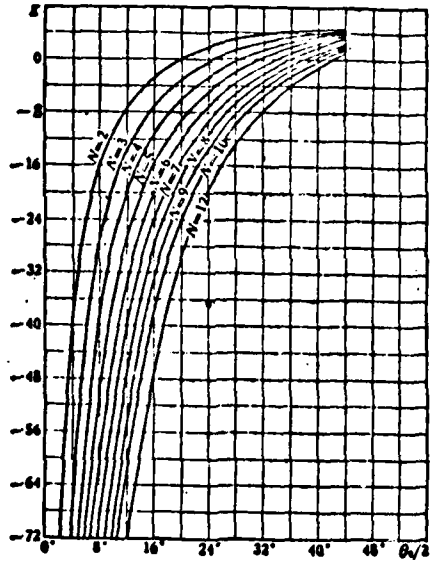

Figure 2. Diagram of functions to compute k.

From this we may obtain V_c/L_p and then substitute ε and N, $\theta_o/2$, k into Equation 12 to get A_{co} and hence Δ. When $\Delta \geqslant 0$, the functions Y_1 and Y_2 corresponding to ε may be obtained from Equation (21) and s_o and A_t which are obtained for Equations (2) and (8). A series of functions Y_1 and Y_2 of ε may be obtained in this way. The solution ε solution of Equation (20) is given by the abscissa of the point of intersection of the decreasing function

Y_1 and increasing function Y_2 of ε. The angular coefficient of the grain can then be obtained; the vertical coordinate is the A_{b01} of the grain. s_{min}/l is found from Figure 3 by using (N, $\varepsilon_{solution}$). As before, we may calculate the grain length L_p and V_c/L_p, A_{co}, Δ, A_1, s_0 , etc. V_c/L_p is the value of A_{c01}.

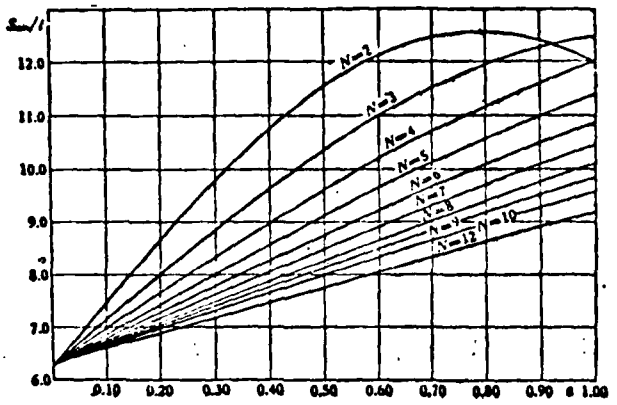

Figure 3. Diagram of the function s_{min}/l.

We then calculate f_1 and R_{ot} from the following two equations:

$$f_1 = \sqrt{\frac{2\Delta}{2\pi - k}} \tag{24}$$

$$R_{ot} = \csc\frac{\theta_0}{2}\left[l\sin\left(\frac{\theta_0}{2} - \varepsilon\frac{\pi}{N}\right) + l + f_1\right] - f_1 \tag{25}$$

When $f_1 = 0$, we know from Equation (14) that whenever $\varepsilon < \varepsilon_{N\mu p}$ then certainly $R_o > 0$, and when $f_1 \neq 0$, then if the equation has a solution, $R_{o1} > 0$. Furthermore, the smaller is $\theta_o/2$, the larger is R_{o1}.

Discussions on the solution:

When we vary ε and $\Delta < 0$ is still true, then the equation has no solution and we must change to larger N and smaller $\theta_o/2$. We

can also vary the known parameters such as k_{kp} within allowed limits (Notice: R_{o1} increases when N is large. A_1 decreases when $\theta_o/2$ is large. When necessary, we may adjust values of N and $\theta_o/2$).

By now all the geometric parameters of internal burning grain has been found. Finally, for the law governing the variation of the combustion surface:

$[0, y_{\theta_0/2}]$ is the first stage of combustion, i.e., the linear stage

$$y_{\theta_0/2} = \frac{l \sin \varepsilon \frac{\pi}{N}}{\cos \frac{\theta_0}{2}} - l$$

In the interval $[0, f_1]$, we have

$$A_{b1} = [s_0 + kf_1 + 2\pi(y - f_1)]L_p \tag{26}$$

In the interval $[f_1, y_{\theta_0/2}]$, we have

$$A_{b1} = (s_0 + ky)L_p \tag{27}$$

$[y_{\theta_0/2}, W]$ is the second stage of combustion, i.e., the non-linear stage. The variation of A_{b11} may be found readily from Equation (7) using the dynamic angular variable $\theta/2$.

It should be pointed out, in passing, that the statement by F. A. Williams et al in [2]: "In the second stage of combustion, ...the grain is , i.e., A_b increases linearly according to $y = rt$" is not true. During the second stage A_{b11} is non-linear and when $\theta_o/2 < \theta/2$ it is monotonically decreasing at first and then monotonically increasing.

REFERENCES

[1] Vandenkerckhove, Jean A., Internal burning star and wagon-wheel designs for solid propellant grains, AD-258519.

[2] Williams, F. A., Huang, N. C., Barrére, M., Fundmental Aspects of Solid Propellant Rockets, AGARDograph, Ch. IV, § 3.3 (1969), 116.

[3] Barrer, M., Zhomott,A., Vebek,B.F., Vandenkerkkhove,Zh. Rocket engines, Oborongiz. Moscow. 1962, 306-312.

[4] Qian Xuesen. On Interstellar Navigation, Science Publishing House (1963) 77-86.

NUMERICAL COMPUTATION AND ANALYSIS OF THE FLOW FIELD IN A LARGE SHOCK TUBE WITH A VARIABLE CROSS-SECTIONAL AREA*

Li Wen xuan, Wang Jiajun
(Beijing University)

Reference [1] has clarified and explained certain flow characteristics of the new shock wave that exists in shock tubes with violently varying cross-section. These characteristics are what the approximate analysis of Chisnell, Chester, Whitman and others cannot describe because they have restricted that the cross-section changes slowly and that there should not be many strong discontinuities. This paper has taken into consideration the state equation of the explosive gas produced by the combustion of the explosive in the high pressure section as well as the contact discontinuity between the explosive gas and air and also extended the calculation to the whole tube (Figure 1). In order to treat many strong discontinuities, we adopted the difference method with artificial viscosity term q. But different from [1], the Lagrangian coordinates are used in this paper so that the contact discontinuities can be easily treated. Also the head of the major shock wave has little vibrations, occupying only 2-3 grid spacings.

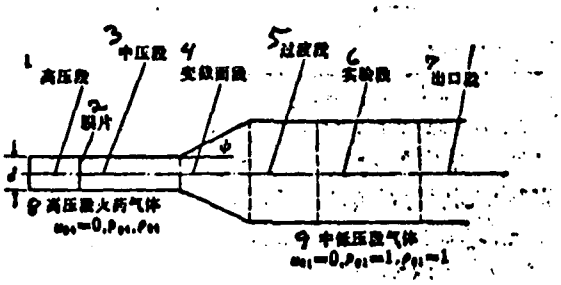

Figure 1. Diagram of the shock tube
Key: 1--high pressure section; 2--film; 3--medium pressure section; 4--section with variable cross-sectional area; 5--transitional section; 6--experimental section; 7--exit section; 8--explosive gas in high pressure section; 9--gas in medium and low pressure sections

* Received February 26, 1978

1. DIMENSIONLESS EQUATIONS AND FINITE DIFFERENCE GRID

The dimensionless equations are

$$\frac{\partial r}{\partial t} = u;\quad \frac{\partial r}{\partial R} = \frac{\rho_0 A_0}{\rho A};\quad \frac{\partial u}{\partial t} = -\frac{A}{\rho_0 A_0}\frac{\partial p}{\partial R};\quad \frac{\partial e}{\partial t} = -\frac{p}{\rho^2}\frac{\partial \rho}{\partial t} \tag{1.1}$$

where p_0, ρ_0 are respectively the static air pressure and the density; d is the diameter of the thin tube; r is the Euler coordinate; R is the Lagrangian coordinate; t is the time; p,ρ,u are respectively the pressure, density and the velocity along the r direction; e is the internal energy; A(r) is the tube cross-sectional area. To make the quantities dimensionless, they have been divided respectively by $d,\ d,\ d/\sqrt{p_0/\rho_0},\ p_0,\ \rho_0,\ \sqrt{p_0/\rho_0},\ p_0/\rho_0,\ d^3$. The subscript 0 denotes the initial values of the various quantities. The difference equations are

$$\frac{r_j^{n+1} - r_j^n}{\Delta t} = u_j^{n+\frac{1}{2}};\quad \frac{r_{j+1}^{n+1} - r_j^{n+1}}{R_{i+1} - R_i} = \frac{\rho_{i+\frac{1}{2}}^0 A_{j,\frac{1}{2}}^0}{\rho_{i+\frac{1}{2}}^{n+1} A_{i+\frac{1}{2}}^{n+1}}$$

$$\frac{u_j^{n+\frac{1}{2}} - u_j^{n-\frac{1}{2}}}{\Delta t} = -\frac{A_j^{n+1}}{\rho_j^0 A_j^0}\frac{[(\delta p)_j^{n+1} + (\delta q)_j^{n+\frac{1}{2}}]}{R_{i+\frac{1}{2}} - R_{i-\frac{1}{2}}}$$

$$e_{i+\frac{1}{2}}^{n+1} - e_{j+\frac{1}{2}}^n = \left(\frac{p_{i+\frac{1}{2}}^{n+1} + p_{j+\frac{1}{2}}^n}{2} + q_{i+\frac{1}{2}}^{n+\frac{1}{2}}\right)\frac{\rho_{i+\frac{1}{2}}^{n+1} - \rho_{j+\frac{1}{2}}^n}{\rho_{j+\frac{1}{2}}^n \rho_{i+\frac{1}{2}}^{n+1}}$$

$$p_{i+\frac{1}{2}}^{n+1} = f(e_{i+\frac{1}{2}}^{n+1},\ \rho_{i+\frac{1}{2}}^{n+1})$$

$$q_{i+\frac{1}{2}}^{n+\frac{1}{2}} = \begin{cases} [c^2(\rho_{i+\frac{1}{2}}^{n+1} + \rho_{j+\frac{1}{2}}^n)/2][(\delta u)_{i+\frac{1}{2}}^{n+\frac{1}{2}}]^2, & \text{当 } (\delta u)_{i+\frac{1}{2}}^{n+\frac{1}{2}} < 0 \text{ 时} \\ 0, & \text{当 } (\delta u)_{i+\frac{1}{2}}^{n+\frac{1}{2}} \geqslant 0 \text{ 时} \end{cases}$$

where

$$(\delta u)_{i+\frac{1}{2}}^{n+\frac{1}{2}} = u_{i+1}^{n+\frac{1}{2}} - u_j^{n+\frac{1}{2}};\quad (\delta p)_j^{n+1} = p_{i+\frac{1}{2}}^{n+1} - p_{i-\frac{1}{2}}^{n+1}$$

$$(\delta q)_j^{n+\frac{1}{2}} = q_{i+\frac{1}{2}}^{n+\frac{1}{2}} - q_{i-\frac{1}{2}}^{n+\frac{1}{2}}$$

c^2 is a constant between 1-4. We take $c^2 = 2$.

Treatment of the initial values $u^{1/2} = u^0 + \frac{1}{2}\Delta t\left(\frac{\partial u}{\partial t}\right)_0 + \frac{1}{2}\left(\frac{\partial^2 u}{\partial t^2}\right)_0\left(\frac{\Delta t}{2}\right)^2 + \cdots$;

Substituting Equation (1.1) as $\frac{\partial u}{\partial t}$, we get

$u_j^{1/2} = u_j^0 - \frac{\Delta t}{2}\frac{A_j^0}{\rho_j^0 A_j^0}\left(\frac{p_{j+\frac{1}{2}}^0 - p_{j-\frac{1}{2}}^0}{R_{j+\frac{1}{2}} - R_{j-\frac{1}{2}}}\right) + O(\Delta t^2)$; the accuracy of $u_j^{1/2}$ is $O(\Delta t^2)$.

The surface separating the two gases is treated with the method of [3]. The advantage of using the Lagrangian coordinates in the calculation is that the surface separating the two gases always lies at the grid point J, thus simplifying the treatment of the surface. At this point, there is discontinuity in ρ,e. Hence, we introduce

$$\frac{1}{\rho_0}\left(\frac{\partial p}{\partial R}\right)_J = \frac{3(p_{J+\frac{1}{2}}^J - p_{J-\frac{1}{2}}^J) - \frac{1}{3}(p_{J+\frac{1}{2}}^J - p_{J-\frac{1}{2}}^J)}{\rho_4\Delta R_2 + \rho_1\Delta R_1},$$

where $\Delta R_1 \Delta R_2$ are respectively the step lengths on the opposite sides of the separating surface; ρ_4, ρ_1 are respectively the initial densities of the explosive gas and air.

Two schemes have been used for the state equation of the explosive gas. In the first state equation, the collisions between hard sphere molecular model of the gas is taken into consideration. Then we take a state equation [2] with two Wylie coefficients. We also adopt from [4] the variable thermodynamic functions: specific heat at constant volume $c_v(T)$, specific heat at constant pressure $c_p(T)$, speed of sound $a_1(\rho_1 T)$, internal energy e(T), etc., but we neglect the chemical reactions that the explosive gas further undergoes after t > 0. The approximation formulae (T being the temperature) for each section of the equation of state are

$$p = 1.108\rho T(1 + 2.5538 \times 10^{-3}\rho + 0.4045 \times 10^{-3}\rho^2);$$

$$e(T) = \begin{cases} 4.0808(T - 3.4344) + 0.1361(T - 3.4344)^2, & 3.4344 \leqslant T \\ 7.4089 + 4.5314(T - 5.1516) + 0.0846(T - 5.1516)^2, & 5.1516 < T \leqslant 6.8688 \\ 15.4399 + 4.8219(T - 6.8688) + 0.0543(T - 6.8688)^2, & 6.8688 < T \leqslant 8.5860 \\ 23.8799 + 5.0086(T - 8.5860) + 0.0377(T - 8.5860)^2, & 8.5860 < T \leqslant 10.303 \\ 32.9517 + 5.1381(T - 10.303) + 0.02861(T - 10.303)^2, & 10.303 < T \end{cases}$$

$$c_v(T) = \begin{cases} 3.6822 + 0.2456(T - 3.4344), & T \leqslant 5.1516 \\ 4.0890 + 0.1524(T - 5.1516), & 5.1516 < T \leqslant 6.8688 \\ 4.3508 + 0.0980(T - 6.8688), & 6.8688 < T \leqslant 8.5860 \\ 4.5193 + 0.0681(T - 8.5860), & 8.5860 < T \leqslant 10.303 \\ 4.6372 + 0.0516(T - 10.303), & 10.303 < T \end{cases}$$

$$e'(\rho, T) = 1.108T\left[1 + \frac{\cdot}{c_v}(1 - 0.2476 \times 10^{-3}\rho^2)\right] \times (1 + 5.1077 \times 10^{-3}\rho + 1.2137 \times 10^{-5}\rho^2)$$

The second kind of state equation uses the perfect gas model with equivalent constant specific heat. We take R = 3.193J/kg, and the absolute thermodynamic index $\gamma = c_p/c_v = 1.225$. After made dimensionless, they become $p = 1.108\rho T$; $e = 4.925T$; $R = 1.108$.

More factors are considered in the scheme of the state equation of the first kind, but more calculations are involved; less factors are taken into consideration for the second scheme, but the calculations involved are simple. The results from the two schemes are close. Especially during the later stages of the motion the results basically overlap. In the complete computational process, the largest difference between the results of the two schemes only appears in the initial stage, and never exceeds 5% (Figure 4). This result deserves attention.

When artificial viscosity is not considered, the stability for a one-dimensional Lagrangian coordinate difference grid is independent of the cross-sectional area A(r), and the Courant condition still holds, i.e., $\Delta t \leqslant \Delta r/a$ [3] . But since the artificial viscosity term is added, in actual computation, we multiply it by the coefficient 0.6, i.e., $\Delta t = \min 0.6 \frac{\Delta r_i}{a_i}$.

2. NUMERICAL RESULTS AND ANALYSIS

Figure 2 shows the distribution of the parameters when the major shock is situated in the middle of the changing cross-section.

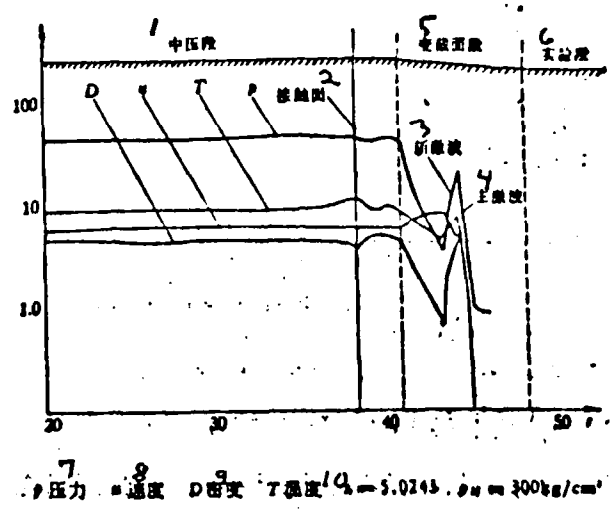

Figure 2. Axial distribution of flow parameters (section with changing cross-section)

Key: 1--medium pressure section; 2--contact surface; 3--section with changing cross-section; 4--new shock; 5--major shock; 6--experimental section; 7--pressure; 8--velocity; 9--density; 10--temperature

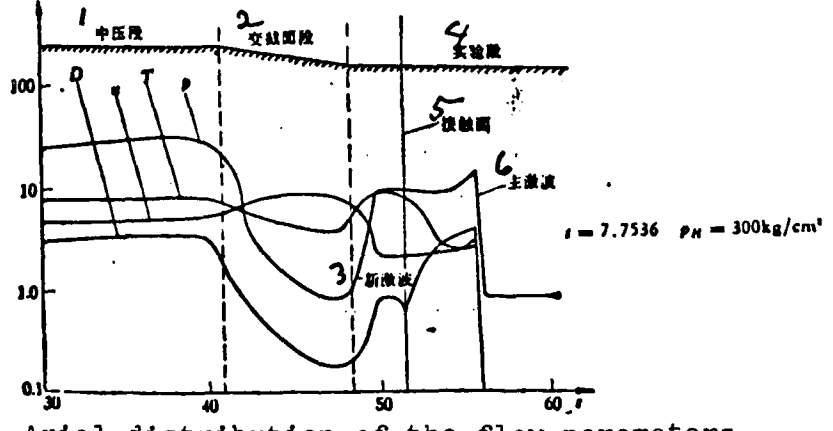

Figure 3. Axial distribution of the flow parameters (experimental section)

Key: 1--medium pressure section; 2--section with changing cross-sectional area; 3--new shock; 4--experimental section; 5--contact surface; 6--major shock

New shock wave appears behind the major shock. The low pressure and low density regions form before the new shock (situated to the left of the major shock) because of the rapid expansion of the gas flow in the conical tube when the separating surface has not yet entered the section with changing cross-section although the major shock is already in the middle of that section. The flow diagram at this time agrees with the analysis in [1].

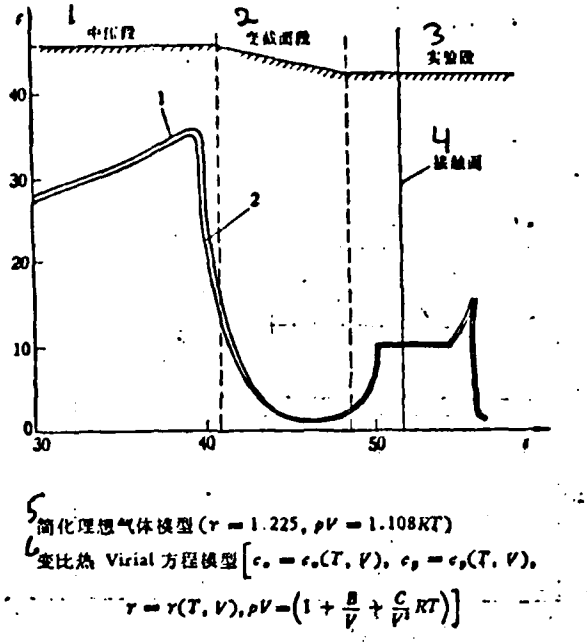

Figure 4. Computational result for the 2 gas models (p_H=300kg/cm^2)

Key: 1--medium pressure section; 2--section with changing cross-sectional area; 3--experimental section; 4--contact surface; 5--simplified ideal gas model; 6--variable specific heat Virial equation model

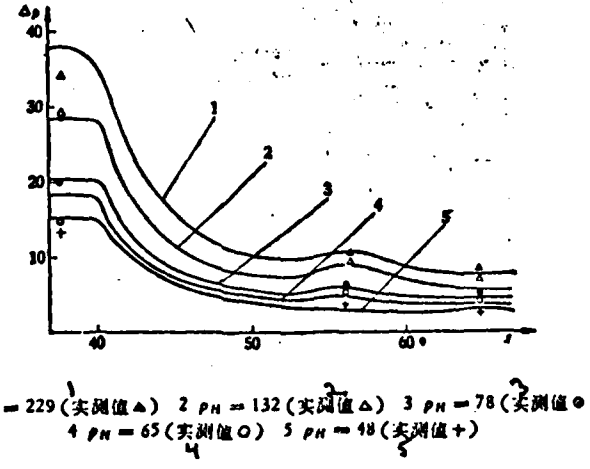

Figure 5. Comparison of calculated peak shock pressure with measured results

Key: 1--experimental measured value; 2--measured value Δ; 3--measured value 0; 4--measured value O; 5--measured value +

Figure 3 is the situation when the major shock, new shock and the separating surface of the gases all are close to the experimental section. The motion of the separating surface of the two gases has already overtaken the new shock when t = 7.75.

From the diagram one can see that to accurately calculate the complete flow field at the experimental position, it is necessary to consider the two-gas media model in front of the changing cross-section. This has not been discussed in [1]. In the work of Chisnell et al, the new shock and the separating surface between the two gases are ruled out. Therefore, it is also not applicalbe for this computation.

Figure 4 are the two pressure curves calculated with the two state equation schemes under the condition that the initial explosive gas excess pressure is 300 kg/cm^2. The two curves basically overlap.

Figure 5 is the comparison between the calculated result and experiment. The calculated result of the peak shock pressure generally differs from the experimental result within 10%.

Figure 6 is the curve of the shock tube pressure that decreases with time. The pressure is calculated at four fixed positions $r = 37.9, 55.0, 57.8, 62.5$ when the initial explosive gas pressure is 100 kg/cm^2. It basically agrees (Figure 7) with the measured pressure curve.

Conservation of total mass and total energy has been used to test the accuracy of the calculation in the whole computational process. When the dimensionless time t = 4.66, the corresponding change in the total mass is 0.34×10^{-2}, and the corresponding energy change is -0.9×10^{-2}.

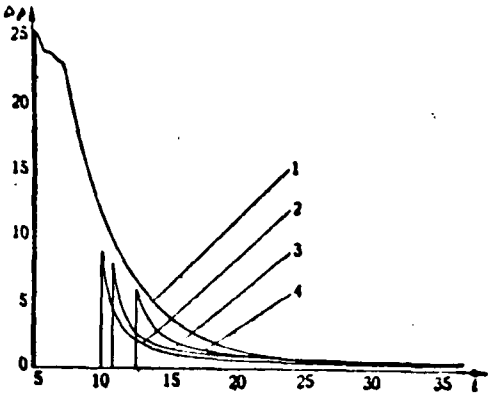

Figure 6. The pressure wave form calculated at four fixed positions when the driving pressure is 100 kg/cm^2

1 $r = 37.9$ 2 $r = 55.0$
3 $r = 57.8$ 4 $r = 62.5$

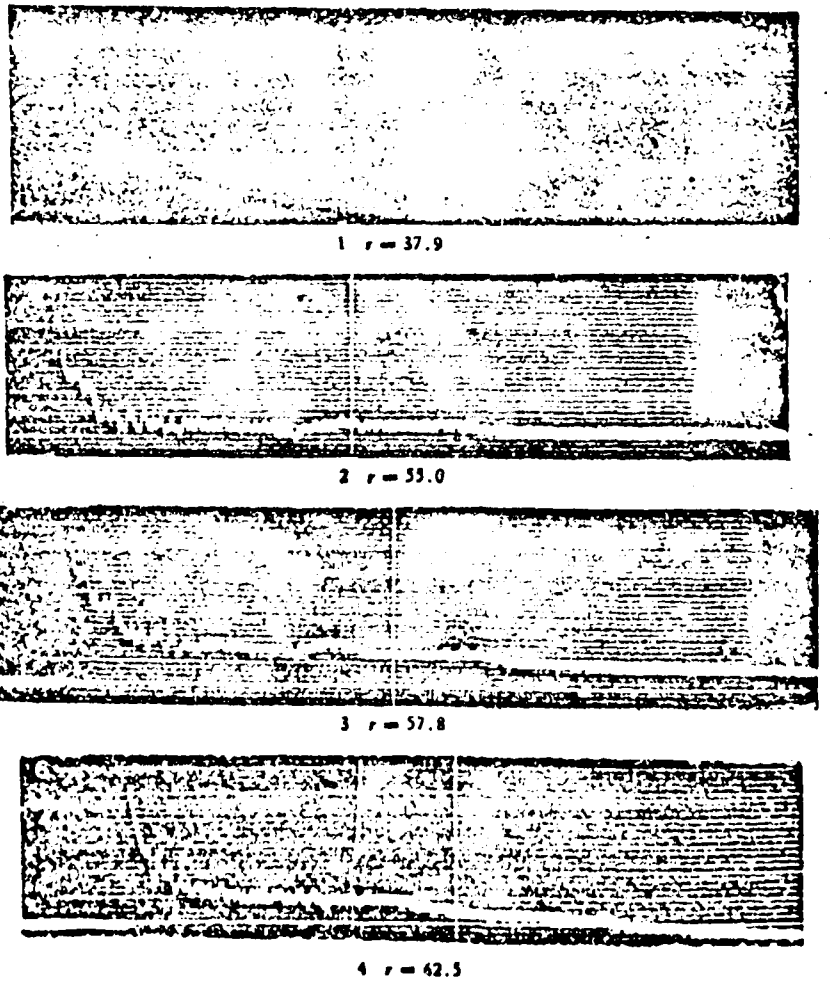

Figure 7. Actually measured pressure wave form

Comrade Zhuang Pengyuan helped us to set up the first state equation scheme. Comrade Huang Duen gave us helpful advice. Comrade Teng Zhenhuan supplied us the test computational data for the case $\gamma = 1.225$. Comrades Wu Jiengwen and Qian Weiyi helped us in organizing the data and preparing the diagrams. To all of them, we extend our thanks.

REFERENCES

[1] Shock wave Computation Group, Beijing University, Chinese Science 6 (1975)

[2] Hisrchfelder, J. O., et al., Molecular Theory of Gases and Liquids (1964).

[3] Richtmyer, R. D., Morton, K. W., Difference Methods for Initial-Value Problems, Interscience Publishers (1967).

[4] Thermodynamic Properties to 6000°K for 210 Substances Involving the First 18 Elements, NASA SP-3001 (1963).

END

DATE
FILMED

11-81

DTIC